TISSUE ENGINEERING
Volume 13, Number 4, 2007

DOI: 10.1089/ten.2006.0321

Small-Diameter Porous Poly (ε-Caprolactone) Films Enhance Adhesion and Growth of Human Cultured Epidermal Keratinocyte and Dermal Fibroblast Cells

JAMES R. MCMILLAN, M.Sc., Ph.D.,[1,2] MASASHI AKIYAMA, M.D., Ph.D.,[1] MASARU TANAKA, Ph.D.,[2] SADAKI YAMAMOTO, Ph.D.,[2] MAKI GOTO, Ph.D.,[1] RIICHIRO ABE, M.D., Ph.D.,[1] DAISUKE SAWAMURA, M.D., Ph.D.,[1] MASATSUGU SHIMOMURA, Ph.D.,[2] and HIROSHI SHIMIZU, M.D., Ph.D.[1]

ABSTRACT

Autologous keratinocyte grafts provide clinical benefit by rapidly covering wounded areas, but they are fragile. We therefore developed biocompatible hexagonal-packed porous films with uniform, circular pore sizes to support human keratinocytes and fibroblasts. Cells were cultured on these porous poly (ε-calprolactone) films with pore sizes ranging from novel ultra-small 3 μm to 20 μm. These were compared with flat (pore-less) films. Cell growth rates, adhesion, migration, and ultrastructural morphology were examined. Human keratinocytes and fibroblasts attached to all films. Furthermore, small-pore (3-5 μm) films showed the highest levels of cell adhesion and survival and prevented migration into the pores and opposing film surface. Keratinocyte migration over small-pore film surface was inhibited. Keratinocytes optimally attached to 3-μm-pore films due to a combination of greater pore numbers (porosity), a greater circumference of the pore edge per unit surface area, and greater frequency of flat surface areas for attachment, allowing better cell–substrate and cell–cell attachment and growth. The 3-μm pore size allowed cell–cell communication, together with diffusion of soluble nutrients and factors from the culture medium or wound substrate. These characteristics are considered important in developing grafts for use in the treatment of human skin wounds.

INTRODUCTION

THERE HAVE BEEN NUMEROUS REPORTS OF micro-scale and nano-scale structured materials with biologically significant properties using basic chemical composition and micro- or nano-scale structural features that may influence cell characteristics grown on these materials.[1–5] Studies examining this phenomenon include those exploring fibrovascular connective tissue cultured on foams,[6,7] osteoblasts grown on porous surfaces,[8,9] tissue fibroblasts on porous membranes,[10] and mouse 3T3 fibroblast-maintained porous collagen–glycosaminoglycan scaffolds.[11] The typical cell responses to nano- and micro-scale structure and geometry include changes in cell adhesion, proliferation, and survival on smaller-scale structures and altered morphology, including cell size, shape, and orientation.[6,7,12,13] Material pore size has emerged as a significant factor affecting cell adhesion and growth on culture substrates; however, the pore shape in many experimental biomaterials has been irregular and had poor uniformity of pore distribution, with variable, generally poorly controlled pore size.[7,10,14,15] We have developed a low-cost process of porous film manufacturing using biocompatible poly (ε-caprolactone) (PCL) material that produces a regular, controlled pore size and a regular, hexagonally packed pore distribution on a flat film.[16–19]

[1]Department of Dermatology, Hokkaido University, Graduate School of Medicine, Sapporo, Japan.
[2]Creative Research Initiative Sousei, Faculty of Science, Hokkaido University, Sapporo, Japan.

Unsupported human skin grafts in current use are composed of keratinocyte sheets and are thin, fragile grafts that must be removed from a donor site, causing further patient injury, and later applied to pre-prepared, cleaned wounded areas to aid rapid wound coverage and achieve effective results. Additional support of these cultured autologous grafts, especially during the handling process, is desirable to improve graft application. Aliphatic polymers such as those made from PCL provide sufficient strength, support, and flexibility and are also biocompatible and biodegradable in the human body. (They are already being used in surgical sutures and blood vessel stents or supports.[13,20]) The porous film also provides an occlusive surface to separate distinct groups of cells on opposite sides; the size of the film pores can precisely control the wound bed connective tissue cells and cultured epithelial cells and the extent to which these two cells types interact.[21] In addition, the center of the pore can itself be used to store or protect biological structures, for example, adhesion components or growth factors encapsulated in controlled-release technologies. Previously, the range of pore sizes that have been regularly and uniformly fabricated has been between 5 and 20 μm in diameter because of limitations in the polymer and solvent used.[19,22,23] Here, we demonstrate that this limit has been extended to grow skin-derived cells on the smallest pores (3 μm) that can be fabricated using self-organizing processes. The precise control of regular pore size limits cell adhesion and communication as well as allowing storage of bioactive compounds provides an important benefit to using the porous films as graft substrates.

We have developed a way to easily and cheaply prepare a regular, patterned surface on which cells can be grown that allow it to be used as a graft to improve wound healing. Our novel porous PCL films (devised and patented by Creative Research Initiative Sousei, Hokkaido University, see patents by Tanaka et al.[1] McMillan et al.[2]) have been tested as a biodegradable platform to support cultures of various human cells.[16,18,24,25] Furthermore, we report here the first fabrication and use of ultra-small-pore-size films with 3-μm-sized pores and report the effects culturing the 2 main skin-derived cells, keratinocytes and fibroblasts, grown on this substrate.

To investigate the effect regular porous films have on monocultures of skin cells, we have investigated the properties of cultured human epidermal keratinocyte and dermal fibroblast cell adhesion, migration, growth, and morphology on different-sized pore substrates. The aim of this study is to enhance our understanding of the processes of cell–substrate interactions and how these factors affect cell adhesion, growth, migration, and morphology. This knowledge will allow us to make further improvements to optimize skin graft efficacy and improve wound healing.

[1]Biodegradable honeycomb films for tissue engineering scaffolds (Patent number: 1999-340568(JP). Application date: 1999/11/30.) Biomedical devices (Patent number: 2001-342484 (JP). Application date: 2001/11/07.)

[2]Porous honeycomb films: applications for cultured human keratinocyte and fibroblast composite grafts and human skin equivalents (Patent number: 2005-188948(JP). Application date: 2005/06/28.)

MATERIALS AND METHODS

Preparation of porous films

The porous PCL uniform 3-dimensional porous films were manufactured using previously described procedures.[16,26,27] Films were disinfected and sterilized (using ethanol and ultraviolet light sterilization), washed, an dair dried, and trapped air was removed using a combination of serial ethanol and sterile 0.1 M Dulbecco's phosphate buffered saline (PBS) washes (Invitrogen/Gibco, BRL, Carlsbad, CA). The sterilized porous films were then directly seeded with monocultures of keratinocytes or fibroblasts. The production procedure uses polymer–solvent mixtures to form perfectly spherical solvent-filled spaces, and thereby pores, in the films. Thus, pore size and depth are intrinsically linked.

Cell sources

The cells (keratinocytes and fibroblasts) were seeded on the upper surface of the film only. Fibroblast cells were sustained in Dulbecco's modified Eagle medium (DMEM) with 10% fetal calf serum, penicillin, and streptomycin (Cambrex, Walkersville, MD) for 24 h to 10 days. Keratinocytes were cultured in keratinocyte growth medium (KGM) I (Cambrex, Walkersville, MD) for between 24 h and 10 days. Normal human neonatal foreskin keratinocytes (Cambrex) were grown in KGM I culture medium (Clonetics, Walkersville, MD) until passage 2 or 3 (P2/P3). The cells were then trypsinized and stored in 10% dimethyl sulfoxide (DMSO) under liquid nitrogen until needed. Normal human dermal fibroblasts were obtained (Cambrex) and grown in DMEM (Cambrex) until P2. Cells were then trypsinized and stored in 10% DMSO under liquid nitrogen until required.

Cell adhesion and growth assays

Normal human neonatal keratinocytes (P2/P3) or dermal fibroblasts (P2) were grown in appropriate culture medium. Cells were trypsinized and counted and 3×10^5 cells plated onto 16-mm-diameter sterilized circular glass-supported substrates including flat (pore-less) PCL film and porous PCL films. This density has previously been determined to be more than sufficient for proper seeding of keratinocyte grafts.[28] Cells were left to adhere for 2 or 24 h to these films with various sized pores. After this time period, the plates were washed 4 times in sterile 0.1 M Dulbecco's PBS and the numbers of live keratinocytes counted after a 5-min incubation with 0.05 μg/mL of acetoxymethyl ester (AME,

C-369), a fluorescent marker for live cells (Molecular Probes, Eugene, OR), in PBS followed by two 5-min washes each in PBS and then DMEM. Only live cells (keratinocytes or fibroblasts) are able to deacetylate the non-fluorescent protein, converting it into fluorescent form. Attached cells were immediately counted using an Olympus Fluoview FV300 confocal and IX70 inverted microscope (Olympus, Tokyo, Japan). Only attached, live, uniformly fluorescent cells were counted on each substrate at a single time point (24 h after initial plating). The mean number of live cells per high power field ($n > 10$) per substrate was calculated. This experiment was repeated 3 times. The treatment groups were compared using one-way analysis of variance (ANOVA) and two sample t-tests using the Minitab statistical package (Minitab Inc., University of Pennsylvania, Philadelphia, PA) at $p < 0.05$ or <0.01 showing significant effects.

For the cell-growth assay, P2-P3 cells were grown on flat or porous films, as previously described,[24] and grown in appropriate culture medium. At specific time points (24, 48, and ≥ 144 h) the plates were washed 4 times in sterile 0.1 M Dulbecco's PBS and the numbers of live cells counted as previously described one directly from phase-contrast photomicrographs. Attached cells were counted using an Olympus IX70 inverted Fluoview FV300 confocal microscope. The numbers of live cells per high-power field ($n > 10$) were calculated per substrate group. Statistical analysis was performed between the treatment groups using one-way ANOVA and two sample t-tests using the Minitab statistical package. The results are shown in Figure 1B and D. This experiment was repeated 3 times.

Migration assay

Normal control P3 keratinocytes or fibroblasts were plated onto substrates (flat calprolactone or porous films). Cells were grown on various substrates in KGM I (keratinocytes) or DMEM (fibroblasts, Clonetics). Cells were grown at between 1×10^5 and 3×10^5 cells per 16-mm well on various substrates as previously described and placed in a temperature- and carbon dioxide (CO_2)-controlled microscopic stage while

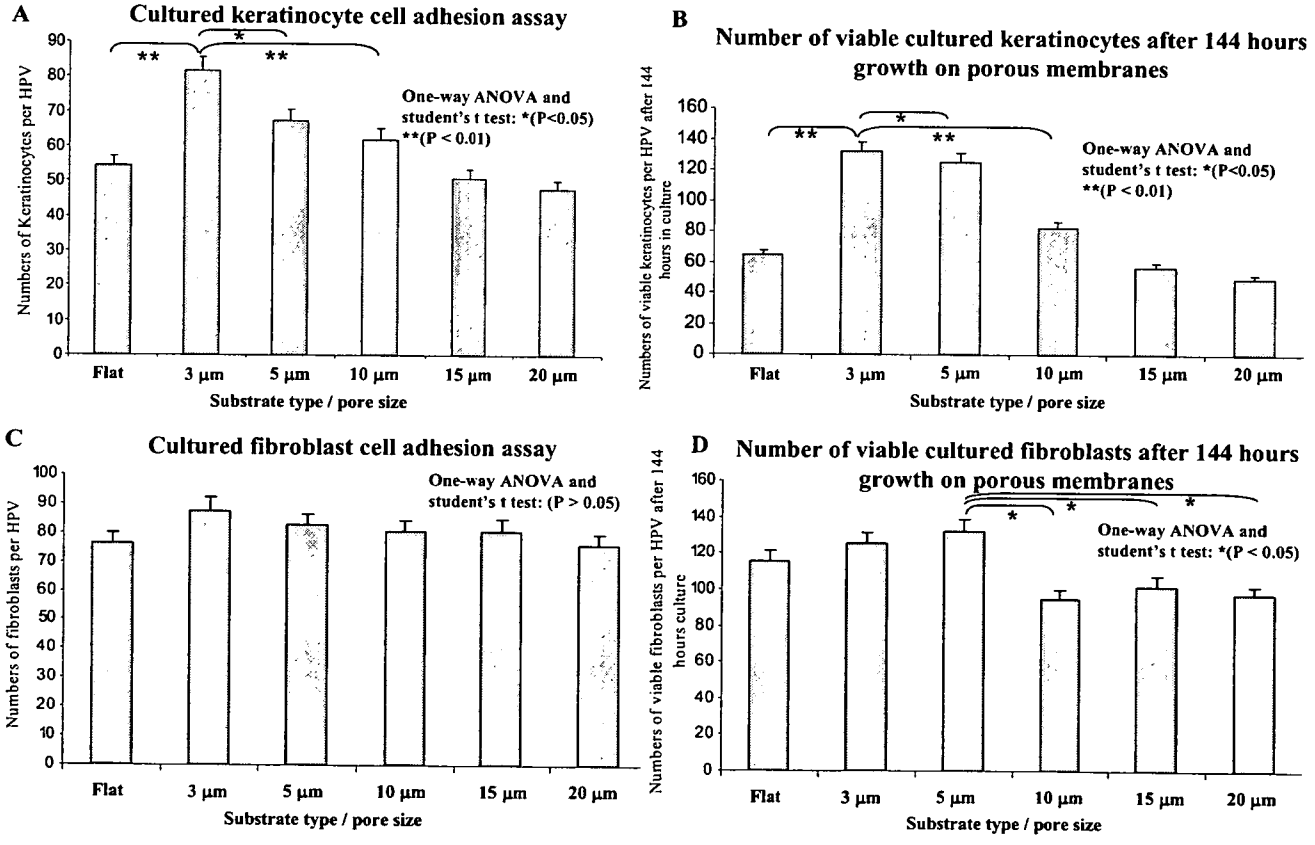

FIG. 1. Keratinocytes show greater increases in cell-substrate adhesion and growth than fibroblasts on porous poly(ε-caprolactone) films. Keratinocyte adhesion assays over 24 h (**A**) demonstrated statistically significantly ($p < 0.01$) greater keratinocyte adhesion between 3 µm porous films than between all other larger films. (**B**) Keratinocyte growth assay over 144 h (6 days) showed a similar ranking but also more-significant differences between 3-µm and other films. Fibroblast adhesion rates over 24 h showed no significant changes when these cells were plated on different films (**C**). (**D**) The fibroblast growth rate over 144 h showed moderate differences ($p < 0.05$) between the flat, 3-µm, and 5-µm group and the larger-pore 10-µm, 15-µm, and 20-µm group. For fibroblasts, the 5-µm films appeared optimal for growth. Statistical analysis: one-way analysis of variance (ANOVA) and Student t tests. *ANOVA, $p < 0.05$, **$p < 0.01$). Error bars 1 = standard deviation.

cells were observed using video microscopy using an INU-NI series microscope stage fitted to an inverted TE 2000 microscope (Nikon, Tokyo, Japan). Single-cell migration assays using time-lapse digital video microscopy were performed for periods of between 8 and 24 h. The number of cells observed using video microscopy was greater than 50 cells per group. Cells were observed using a time-lapse video interval of 5 min, and the distance traveled was observed using a precalibrated scale and MCID/M2 image analysis software (Imaging Research Inc., Ontario, Canada). Cell viability counts were confirmed after 5 min incubation with 0.05 μg/mL of C-369 AME, a fluorescent marker for live cells (Molecular Probes), and examination under a confocal microscope as previously described. The average distance traveled per hour was calculated for each cell type on each substrate. Statistical analysis was performed to compare the treatment groups using one-way ANOVA and two sample t-tests using the Minitab statistical package.

Scanning electron microscopy

Cells grown on various substrates for 48 h were fixed in 2% glutaraldehyde for at least 4 h and processed for routine scanning electron microscopy (SEM). Briefly, samples were dehydrated in a graded ethanol series, treated twice with isoamyl acetate, and critical point CO_2 dried using a Hitachi HCP-2 followed by platinum-palladium sputter coating in a Hitachi E-1030 (Tokyo, Japan). Specimens were examined using a Hitachi S-4500 scanning electron microscope fitted with a digital image capture system. Approximately 200 adherent cells were examined per group.

Transmission electron microscopy

Cells grown on films for 48 h were fixed in 2% glutaraldehyde solution, post-fixed in 1% osmium oxide, dehydrated, and processed for conventional electron microscopic observation according to the methods described previously.[29] Alternatively, samples were dehydrated using a graded ethanol series but were not treated with propylene oxide. Instead they were washed in 100% ethanol and a methanol–acetic acid mixture and subsequently embedded in white acrylic resin (London Resin Company, Reading, UK) or Lowicryl K11M (Ladd Research Industries, Burlington, VT) to avoid harmful film–solvent interactions that were polymerized using ultraviolet light at 4°C for 48 h. Semithin sections were cut and stained with Richardson's stain.[30] Samples were cut, stained with uranyl acetate and lead citrate, and viewed under a Hitachi H-7100 transmission electron microscope at 75 kV.

Confocal immunofluorescence microscopy

Indirect immunofluorescence was performed as previously described[29] using 3-μm porous films with keratinocyte and 5-μm porous films and fibroblast monocultures in addition to cryostat normal skin sections. The mouse monoclonals M3F7 and LH7:2, recognizing collagen IV and collagen VII, respectively, were used at neat and 1 in 2 dilutions.[29] M3F7 were obtained from the Developmental Studies Hybridoma bank, University of Iowa. A laminin 5 antibody, GB3, directed against the laminin 5 α2 chain (Harlan Sera Laboratory, Loughborough, UK), mouse immunoglobulin (Ig)G vinculin VIN-11-05 (Sigma, St Louis, MI) 1 in 100 dilution, desmoplakin (11F5) used at 1 in 50 dilution, and E cadherin HECD1 were used. 4C7 monoclonal antibody recognizing the laminin 10 was used diluted 1 in 25.[29] The following primary antibodies and sera were also used in this study: anti-human keratin 14, clone LL001 diluted 1 in 2 (gifts from B. Lane, Dundee, UK), anti-talin, TD77 mouse antibody diluted 1 in 200, mouse anti-collagen I (1 in 100), and rabbit polyclonal vimentin diluted 1 in 200 (Abcam, Cambridge, UK) against synthetic talin (amino acids 2269-2541) encoding the polypeptide f actin binding region. Staining for actin was performed using phalloidin and rabbit anti-human actin rabbit IgG antisera (Biomedical Technologies, Stoughton, MS).

Cell and film cryostat sections were fixed in acetone methanol and incubated with primary antibodies and antisera. Sections were incubated with secondary antibodies conjugated to fluorescein isothiocyanate (FITC; rabbit anti-mouse IgG or goat anti-rabbit IgG; 1:200; Dako, Tokyo, Japan). Sections were then labeled with a Topro 3 nuclear counterstain (Jackson Immuno-Research, West Grove, PA, diluted 1 in 20,000). The sections were examined using an Olympus Fluoview FV300 confocal microscope. Controls included normal skin cryostat sections, with PBS substituted for the primary antibody, myeloma supernatant, or an irrelevant immunoglobulin isotype as a negative control. All experiments were performed at least twice.

RESULTS

Cell adhesion and growth assays

Cell adhesion on porous films. Keratinocytes (Fig. 1A) and fibroblasts (Fig. 1C) were able to attach to, adhere to, and grow on all porous films. The initial adhesion of keratinocytes (over 24 h) was greater on the small-diameter porous films (with 3 μm producing the best results, closely followed by the 5-μm, 10-μm, 15-μm, and 20-μm porous films, see Fig. 1A). Keratinocyte adhesion was greatest using the smaller-diameter porous film pores (with 3 μm producing the best results, followed closely by the 5-μm film, Fig. 1). However, overall, cell adhesion to the porous films was significantly greater in human dermal-derived fibroblasts than in human epidermal keratinocytes (Fig. 1A vs 1C). Fibroblasts, overall, showed far less-significant differences (Fig. 1C, $p > 0.05$) between adhesion rates on different films, with only a slight increase in adhesion 3 μm compared to sequential minimal decreases in 5 μm, 10 μm and flat surfaces. These data are in broad agreement with our previous

report that demonstrated high levels of adhesion to various porous films shown by the mouse NIH 3T3 fibroblast cell line.[24]

Cell growth rates. Cell growth rates were assessed for up to 6 days. All culture samples were seeded with the same number of cells on each substrate in each well. After 6 days of culture, live cells were stained and cells counted per randomly selected high-power field. Keratinocytes showed the highest proliferation and/or survival rates on 3-μm porous films, although the 5-μm porous films also demonstrated a slightly slower growth rate. These two samples' growth rates were significantly higher than those of any of the larger-pore films (10 μm > 15 μm > 20 μm) or flat substrate.

Fibroblasts showed similar, high growth levels on the 5-μm and 3-μm pore films and flat substrates. However, they also showed significantly lower growth rates on the larger-pore films (10-μm, 15-μm, and 20-μm pores) than on those with smaller pores. This was an approximately 25% to 30% lower growth rates on films with 10-μm pores than on those with 5-μm pores.

Cell migration over the film surface

Lateral cell migration over the surface of the porous film was analyzed using time-lapse video and image analysis and showed that keratinocyte migration rates were lower after plating of cells onto any PCL film than for keratinocytes grown on plastic[31] (Fig. 2, grey bar flat (poreless) PCL vs porous PCL films). Fibroblast migration was significantly less ($p < 0.05$ and $p < 0.01$) but not completely inhibited after plating on porous films, causing reductions of up to 30% (Fig. 2 white bars flat PCL vs 3-μm and 5-μm PCL film, respectively). The differences here reflect severely slower keratinocyte migration rates on any PCL film than the reported migration of keratinocytes on plastic[31] and gradually slower migration rates of fibroblasts grown on 3-μm and 5-μm films (respectively) than for those grown on pore-less flat films.

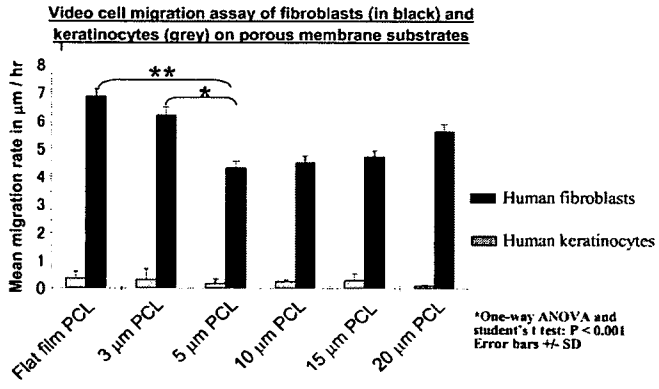

FIG. 2. Video microscopy–assessed migration showed higher migration rates for fibroblasts than for keratinocytes when maintained on porous films. Keratinocyte migration was inhibited on porous membranes, whereas fibroblasts showed the highest migration rates on flat pore-less films, only moderate reductions in migration on 3-μm films and more significant reductions on 5- to 10-μm films. Surprisingly fibroblast migration showed a modest increase on the 20–μm films. Statistical analysis: one-way analysis of variance and Student t tests. $*p < 0.05$, $**p < 0.01$). Error bars 1 = SD.

Migrating cells can cross films with smaller pore sizes more easily than they can cross films with large pores. In addition, the length of pore edge per specific unit surface area is greatest in the small-pore film, which enables cells to use plasma membrane lamleopodia extensions (presumably containing focal contacts) to gain better adhesion on the underlying surface and allow better signal transduction that enable still better adhesion and growth.

Scanning electron microscopy

Keratinocytes seeded onto flat pore-less surfaces attached quickly, spread, and flattened within 2 to 4 h of plating (and were examined using phase contrast microscopy). Cells attached to the underlying substrate using thin filopodial extensions of the plasma membrane that resembled focal adhesions (Fig. 3A–D, white arrows). Keratinocytes subsequently formed small colonies of cells that grew and migrated over the flat films. Keratinocytes on all sizes of porous substrates (Fig. 3B–D) took longer than 48 h to spread (Fig. 3B). Keratinocytes seeded near adjacent cells or those that produced daughter cells after mitotic division maintained desmosome connections (white arrowheads in Fig. 3C) between adjacent cells. Cells were typically positioned over adjacent pores (see Fig. 3B, C). Ultimately, keratinocytes plated on films with pores of any size spread and flattened, covering the film surface with a diameter of as much as 30 to 40 μm (Fig. 3D). Eventually, keratinocytes characteristically formed thin, flat, "fried egg" shapes that covered the pores and surface of the film in equal proportion (Fig. 3D). On the largest-pore films (15–20 μm) occasional individual keratinocytes could be seen within the pores of the film (data not shown).

Fibroblasts grown on flat films quickly attached, spread, and flattened within 3 h (Fig. 3E). Fibroblasts on porous films spread more slowly than on flat films and initially maintained an elongated shape but without significant flattening (Fig. 3F vs E). Eventually, fibroblasts spread and formed flattened shapes covering the porous films as the number of cells increased (Fig. 3G). In larger-pore films (≥5 μm), entire cells were observed that had entered pores, and the cell body passed into the pore space between the upper and lower layers of the film (Fig. 3H, inset). Fibroblasts, because of their thinner, more-elongated shape, were much more frequently observed entering the large film pores (Fig. 3H and inset) than keratinocytes.

Transmission electron microscopic analysis of cells grown on support films

Transmembrane cell migration keratinocytes. Semithin sections showed the basically normal morphology of keratinocytes and fibroblasts grown on flat and porous film supports

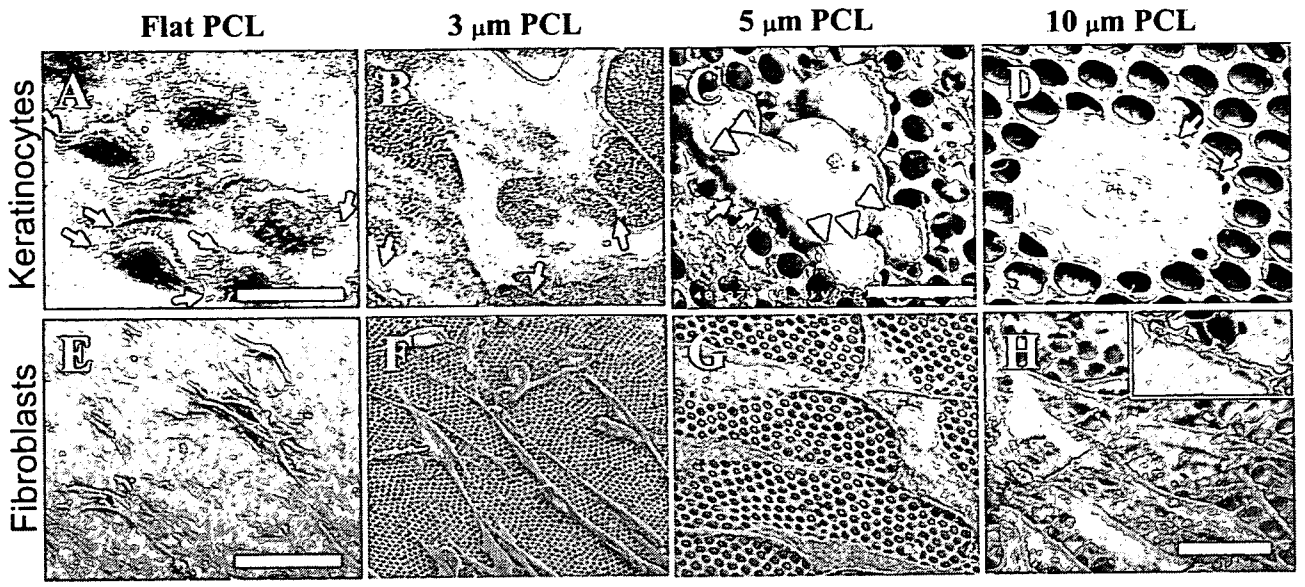

FIG. 3. Scanning electron micrographs showing the morphology of cells grown on flat and porous films after 48 h in culture. Keratinocytes (**A–D**) and fibroblasts (**E–H**) exhibit good cell–substrate attachment on all the surfaces by means of cell projections (filopodia) attaching to the surfaces (arrows in **A**). These cell projections resembled focal adhesion associated lamellipodia/filopodia (arrows in **A–D**). Keratinocytes were slower to spread than fibroblasts but formed flatter, more-rounded cells (**B–D**). Adjacent keratinocytes were able to form close cell–cell associations at possible sites of cell-junction formation (arrowheads in **C**). Conversely, fibroblasts formed small round cells but rapidly (in <1 h) elongated becoming spindle-like cells containing nuclear bulges eventually becoming 25 μm in length. On larger porous films with pores 10 μm and greater, cell processes and entire fibroblasts entered the pores (see inset in **H**). Scale bars (**A, C, E**) 15 μm, (**B, D, F, G, H**) 30 μm.

(Fig. 4A–J). The black dashed lines highlight the upper surface of the flat or porous film (Fig. 4A–J). Keratinocytes seeded on porous films initially showed a rounded morphology and typically sent down small cytoplasmic projections extending 1 to μm into the pores (arrows in Fig. 4C, E, G, I). The number of pores per unit surface area were highest in small-pore (3 μm, Fig. 4C) films and lowest on the large-pore films (15 μm, Fig. 4I; 20 μm, Fig. 4K). (For review of porous film properties, see[22].) This means that keratinocytes grown on small-pore film could form greater numbers of cell projections into the pores per unit surface area than in larger-pore films. In the large-pore films, entire necrotic keratinocytes with pyknotic nuclei were observed within the open pore spaces (Fig. 4K, arrows).

As previously demonstrated using SEM, fibroblasts grown on all porous films showed a flatter morphology than keratinocytes (Fig. 4B). Fibroblasts were also able to extend variable length cell processes and entire cells into the pores, but because these cells were generally longer and thinner than keratinocytes, entire cells were able to enter any pores larger than 5 μm (arrows in Fig. 3F, H, J, L). As the pore size increased beyond 5 μm, increasing numbers of fibroblasts were able to migrate and multiply in the center of the porous films (Fig. 3F, H, J, L).

Transmembrane cell migration. The transmembrane migration of keratinocytes was completely prevented using films with smaller-diameter pored (with the 3- and 5-μm films most effectively preventing transmigration). Only the smallest-pore (3 μm) films were effective at preventing the transmembrane transfer of migrating fibroblasts cells into the spaces in the center of the film. The ratio of pore-size diameter to minimum cell diameter is an important property in determining the extent of cell transmembrane migration into the pores and their subsequent migration to the other side of the porous film. The use of small-pore films might therefore prove advantageous in a graft to avoid the transmembrane transfer of different cell types.

Keratinocyte ultrastructure

Ultrastructure of individual keratinocytes grown on flat and porous films showed a 3- to 4-cell multi-layered but incompletely keratinized epidermis, typical of cells maintained in submerged culture (keratinocytes seeded on 5-μm film Fig. 4M, N). At the apical surface, there were numerous villus-like structures and linking adjacent keratinocytes. There were electron-dense desmosomal plaques associated with keratin intermediate-filament bundles (Fig. 4N, white arrow and inset). At the basal pole of the cultured epidermis, there were severely disorganized keratin filaments, but no basal lamina or well-formed hemidesmosome structures were present (Fig. 4M). Small, hypoplastic hemidesmosomes were occasionally observed along the basal pole but were not attached or associated with any external or underlying structures. Sub-basal dense plates were not observed on

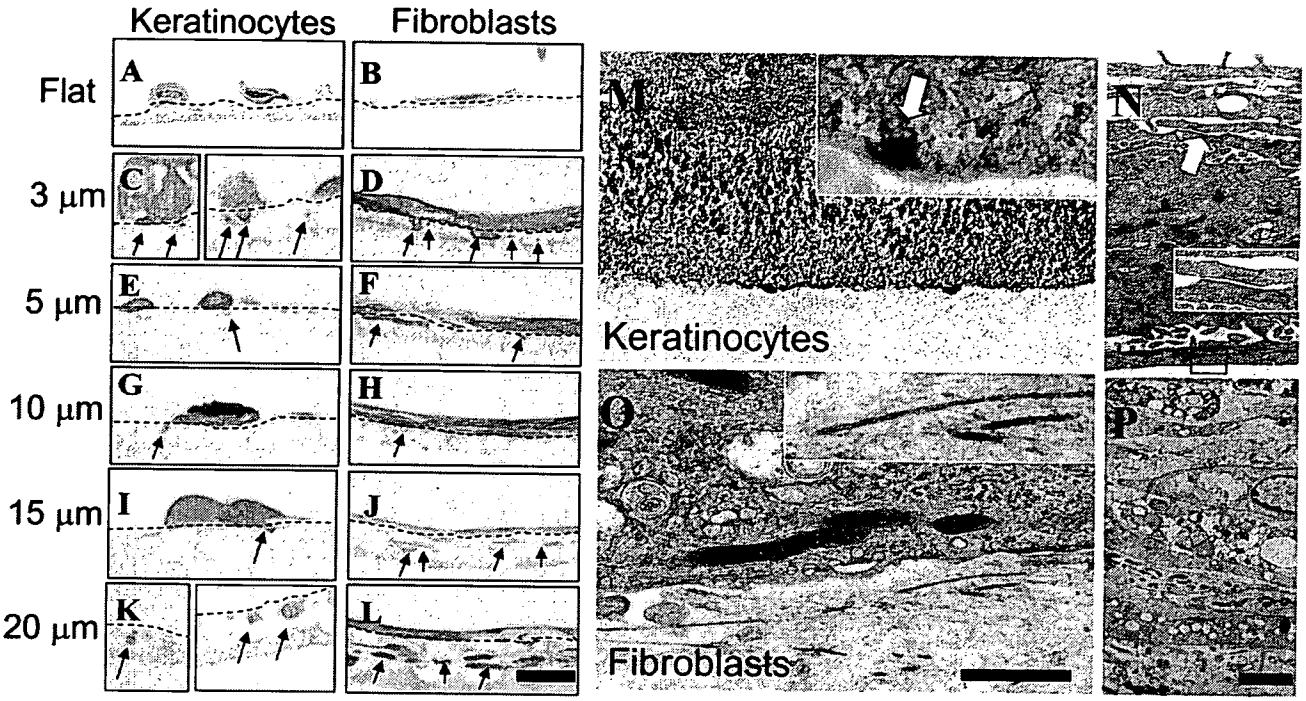

FIG. 4. Semithin and transmission electron microscopy shows the cell morphology, position, and ultrastructure of cells grown on porous films. The dotted lines (**A–J**) highlight the upper surfaces of the films. Both cell types grown on small-pore films (**A–D**, 3-5 μm, arrows) produced filopodial cell projections into the pore space. Furthermore, keratinocytes grown on larger pores (10- to 20-μm-sized pores, **E–J**, arrows) formed larger processes, and on the 20-μm pores, the keratinocytes entered the pore (see arrows in **I**). Often these isolated cells showed pyknotic nuclei and failed to survive (**I**). Fibroblasts were generally longer than even the largest pore size and entered pore sizes greater than 10 μm. The histology of keratinocyte (**H**) and fibroblast (**I**) long-term cultures maintained for 3 weeks shows multiple layers of cells. Ultrastructural analysis of keratinocytes showed no basal lamina or properly formed hemidesmosomes (**M**, arrows, inset in **M**). However, multiple intermediate and microfilaments were observed overlying the keratinocyte plasma membrane (**M, N**). Desmosomes were also seen between keratinocytes (white arrows in **N**, inset). Fibroblasts formed thin, elongated stacks of active cells containing vesicles and mitochondria and collagen fibers between adjacent cells. Scale bar 10 μm (**A–L**), 100 nm (**M, O**), 1 μm (**N, P**). Color images available online at www.liebertpub.com/ten.

any hemidesmosomes. A significant number of substratum-associated actin microfilament bundles were observed at the base of the basal layer keratinocytes (Fig. 4M) and in cell processes (data not shown).

Fibroblast ultrastructure

The ultrastructure of fibroblasts grown on 5-μm porous films showed heterogeneous layers of closely and loosely packed fibroblasts (Fig. 4O, P). Fibroblast morphology was generally that of active cells containing numerous secretory and endocytotic vesicles and together with numerous organelles (Fig. 4P). Cultured fibroblasts typically formed between 2 and 4 cell layers, in which the cells were closely packed or contained intercellular spaces filled with extracellular matrix, ground substance, and cross-banded collagen fibers (Fig. 4O, inset). A significant amount of substratum-associated actin microfilament and (presumably vimentin) intermediate filament bundles were observed within the fibroblasts (Fig. 4O) and in cell processes (data not shown).

Confocal fluorescence microscopy

Keratinocytes cultured on 3-μm films stained with keratin 14 and at the cell borders with the cell adhesion markers desmoplakin and E-cadherin. Keratinocytes showed bright staining for the focal contact and adhesion associated antigens vinculin, actin, and vitronectin but not for the epidermal matrix proteins or the hemidesmosomal anchoring filament protein laminins 5 (332), laminin 10/11 (511 or 521), collagen I, or collagen IV. Collagen VII and fibronectin showed weak epidermal cytoplasmic staining but no evidence of matrix deposition on the film.

Fibroblasts cultured on 5-μm films stained with vimentin (not keratin) and at the cell borders and extracellularly with fibronectin, vitronectin, and collagen I. Fibroblasts showed normal, bright cytoplasmic staining for the focal contact-associated antigens vinculin and actin and weaker staining for talin but no staining for the epidermal matrix proteins laminins 5(332), laminin 10 (511), collagen I, or collagen IV. Collagen VII showed weak cytoplasmic staining with no evidence of matrix deposition on the film.

DISCUSSION

Keratinocytes and fibroblasts adhere to, spread on, and can grow and survive on flat and all sizes of regular, hexagonally packed porous (ε-calprolactone) films with pores ranging in size from 3 to 20 μm. Specifically, we have demonstrated that keratinocyte attachment is dependent on the size of the pores and that cell adhesion was highest on the smallest 3-μm films. The unique characteristics of the porous patterned films account for these changes in the 2 cell types studied. Each cell type displays subtle differences due to their particular adhesion and growth characteristics, as shown by their unique repertoire of cell-adhesion receptors and cell–cell interactions with porous substrates.

Substrate characteristics, temperature, the presence of cations,[32] cell activation state, and cell viability, which is modulated by cytokines, govern keratinocyte adhesion in part. Keratinocytes in our study were more discriminating than fibroblasts and adhered best on smaller-pore-sized film (3-μm-pored films), the next best adhesion pore size being 5-μm-pore film. The explanation for these effects comes after several observations. First, if this pore size is greater than the size of the initial seeded cells, they can and do enter the film pores. Because keratinocytes require direct adjacent cell–cell contact for proper levels of growth, signaling, and cell survival, cell separation caused by the larger pores is likely to detrimentally affect these processes. It has previously been shown that keratinocytes seeded onto grafts without proper cell–cell and cell–substrate contact fail to form appropriate epidermal sheets[33] and survive in culture.[28,33] Further beneficial characteristics of the small-pore films include the fact that they have a greater surface area over which cells can adhere. Finally, the smaller pore size produces a greater length of pore edge per surface area that cells can insert their plasma membrane lamelapodia and filopodial extensions into to gain leverage and increase cell adhesion. This leverage may also inhibit cell migration. Keratinocytes require cell–cell and cell–substrate contact especially for cell growth and survival. When cells, especially keratinocytes, become isolated or removed from adjacent cell–cell contact (or are trapped in pores) readily undergo cell cycle arrest or apoptotic changes,[34] as was seen with pyknotic cells in our growth experiments. Similarly, mutations in the first human genetic disease affecting focal contact-adhesion protein kindlin-1 in skin also cause premature keratinocyte cell death by apoptosis and skin thinning and erosions.[35–37]

Our data suggest that the most important keratinocyte adhesive mechanism does not involve the proper formation of the hemidesmosome junction or the assembly of any extracellular components, including laminins 5/10[29] or matrix secretion of collagens I, IV, and VII. Conversely, fibroblasts and keratinocytes that adhered to porous films assembled highly dynamic, actin-associated focal adhesion-like structures that were observed attaching to the surface of the films. Given the short time frame over which cells, particularly fibroblasts, adhered to and spread on the films and taken together with the abundance of cytoplasmic actin filaments and focal adhesion components observed within filopodia and lamelapodia, we suggest that focal adhesions form the majority of adhesive junctions on these surfaces. The identification of fibronectin and vitronectin deposits in cultures and recent findings of the importance of focal contacts and their associated proteins on the adhesion of other cell types cultured on porous membranes further supports this hypothesis.[19,38,39]

Closely related to the film adhesive characteristics is the related ability to allow cell migration. The ability of the cells to gain leverage because of the extra length of pore edge or to enter the film pores in the small-pore samples probably affected keratinocyte and fibroblast migration rates, as previously mentioned. Our findings support previous reports that fibroblast migration on collagen sponges with various size pores was significantly greater than that of keratinocytes.[40]

In addition, we demonstrated that the smallest, 3-μm pore size was most efficient at inhibiting the transmigration of both cell types (to the opposite side of the film). Cell transmigration has important future implications in the design of monolayer or bilayer polymer grafts for the treatment of skin wounds. The beneficial adhesive properties and blocking of transmigration of the smaller pores will prove to be an important factor when this film is used to support a bilayered human skin equivalent or dermal equivalent by preventing two different cells types from mixing.

Keratinocytes are more selective than fibroblasts and grow best on small pore-sized film (3-μm-pored films). The second most effective film size for keratinocyte adhesion was the 5-μm film ($3\,\mu m > 5\,\mu m > 10\,\mu m >$ flat $>> 15\,\mu m < 20\,\mu m$). Explaining these growth effects on both cell types encompasses cell substrate adhesion and ability to migrate and form cell–cell contacts that all contributed to affect *in vitro* growth rates.[41] Our data suggested that the keratinocytes were more likely to grow poorly in isolation or in small colonies without significant all-round cell–cell contact. This would have important implications for cell contact–induced growth signals.[42,43] Other reports have also indicated that keratinocytes were more likely to grow poorly in isolation without cell–cell contact similar to that seen on porous collagen sponges.[40] Fibroblasts grew equally well on flat or small-pore-sized film but on pores larger than 10 μm showed significantly slower grow rates. Direct migration of fibroblasts on the underlying substrate was relatively short term due to formation of multiple cell layers. However, fibroblast adhesion and growth-signaling mechanisms are known to involve many of the same actin-associated focal-adhesion molecules as in keratinocytes.[44–46] NIH 3T3 fibroblasts have previously been demonstrated to adhere to all sizes of porous films.[24]

The important characteristics of porous films that cause significant changes in cell adhesion, migration, and growth rates include characteristics that enable cells to extend focal-contact plasma-membrane projections to gain adhesion and leverage that allow better growth. Further work is required to

describe the properties of PCL films with smaller pores and to determine whether further beneficial effects of adhesion, growth, and increases in keratinocyte migration rates that are observed in culture are maintained in *in vivo* wound-healing models.

ACKNOWLEDGMENTS

We thank Ms. Y. Miyamura and Ms. N. Ikeda for their excellent technical assistance in cell-film preparation, Mr. H. Nakamura and Ms. K. Sakai for their electron microscopy assistance, and Ms. Y. Morita and Ms. E. Ito for their excellent technical assistance in film fabrication and help with the migration studies. This work was supported by a grant-in-aid from the Health and Labor Sciences Research Grant (research into Human Genome, Tissue Engineering) H17-Saisei-12 (to J.R.M.) and by a grant-in-aid of Scientific Research A (17209038, H.S.) from the Japanese Society for the Promotion of Science. This work was also supported by a Health and Labor Sciences Research Grant (Research into Measures Treating Intractable Diseases) from the Ministry of Health, Labor and Welfare (H16-Nanchi-05, to H.S.) and a Project for Realization of Regenerative Medicine from the Ministry of Education, Science, Sports, and Culture of Japan (to H.S.). The hybridoma monoclonal antibody supernatants were obtained from the Developmental Studies Hybridoma Bank, developed under the auspices of the National Institute of Child Health and Development and maintained by the Department of Biological Sciences, University of Iowa, Iowa City, Iowa.

REFERENCES

1. Stenzel-Rosenbaum, M.H., Davis, T.P., Fane, A.G., and Chen, V. Porous polymer films and honeycomb structures made by the self-organization of well-defined macromolecular structures created by living radical polymerization techniques. Angew Chem Int Ed Engl **40,** 3428, 2001.
2. Zein, I., Hutmacher, D.W., Tan, K.C., and Teoh, S.H. Fused deposition modeling of novel scaffold architectures for tissue engineering applications. Biomaterials **23,** 1169, 2002.
3. Chung, T.W., Yang, M.G., Liu, D.Z., Chen, W.P., Pan, C.I., and Wang, S.S. Enhancing growth human endothelial cells on arg-gly-asp (RGD) embedded poly (epsilon-caprolactone) (PCL) surface with nanometer scale of surface disturbance. J Biomed Mater Res A **72,** 213, 2005.
4. Serrano, M.C., Pagani, R., Vallet-Regi, M., Pena, J., Ramila, A., Izquierdo, I., and Portoles, M.T. *In vitro* biocompatibility assessment of poly(epsilon-caprolactone) films using 1929 mouse fibroblasts. Biomaterials **25,** 5603, 2004.
5. Ng, K.W., Khor, H.L., and Hutmacher, D.W. *In vitro* characterization of natural and synthetic dermal matrices cultured with human dermal fibroblasts. Biomaterials **25,** 2807, 2004.
6. Wake, M.C., Gupta, P.K., and Mikos, A.G. Fabrication of pliable biodegradable polymer foams to engineer soft tissues. Cell Transplant **5,** 465, 1996.
7. Wake, M.C., Patrick, C.W., Jr., and Mikos, A.G. Pore morphology effects on the fibrovascular tissue growth in porous polymer substrates. Cell Transplant **3,** 339, 1994.
8. Lee, S.J., Choi, J.S., Park, K.S., Khang, G., Lee, Y.M., and Lee, H.B. Response of mg63 osteoblast-like cells onto polycarbonate membrane surfaces with different micropore sizes. Biomaterials **25,** 4699, 2004.
9. Wan, Y., Wang, Y., Liu, Z., Qu, X., Han, B., Bei, J., and Wang, S. Adhesion and proliferation of oct-1 osteoblast-like cells on micro- and nano-scale topography structured poly(l-lactide). Biomaterials **26,** 4453, 2005.
10. Berry, C.C., Campbell, G., Spadiccino, A., Robertson, M., and Curtis, A.S. The influence of microscale topography on fibroblast attachment and motility. Biomaterials **25,** 5781, 2004.
11. O'Brien, F.J., Harley, B.A., Yannas, I.V., and Gibson, L.J. The effect of pore size on cell adhesion in collagen-gag scaffolds. Biomaterials **26,** 433, 2005.
12. Lee, S.H., Kim, B.S., Kim, S.H., Choi, S.W., Jeong, S.I., Kwon, I.K., Kang, S.W., Nikolovski, J., Mooney, D.J., Han, Y.K., and Kim, Y.H. Elastic biodegradable poly(glycolide-co-caprolactone) scaffold for tissue engineering. J Biomed Mater Res **66A,** 29, 2003.
13. Jeong, S.I., Kim, S.H., Kim, Y.H., Jung, Y., Kwon, J.H., Kim, B.S., and Lee, Y.M. Manufacture of elastic biodegradable plcl scaffolds for mechano-active vascular tissue engineering. J Biomater Sci Polym Ed **15,** 645, 2004.
14. Wald, H.L., Sarakinos, G., Lyman, M.D., Mikos, A.G., Vacanti, J.P., and Langer, R. Cell seeding in porous transplantation devices. Biomaterials **14,** 270, 1993.
15. Choi, Y.S., Hong, S.R., Lee, Y.M., Song, K.W., Park, M.H., and Nam, Y.S. Studies on gelatin-containing artificial skin: II. Preparation and characterization of cross-linked gelatin-hyaluronate sponge. J Biomed Mater Res **48,** 631, 1999.
16. Tanaka, M., Takebayashi, M., Miyama, M., Nishida, J., and Shimomura, M. Design of novel biointerfaces (II). Fabrication of self-organized porous polymer film with highly uniform pores. Biomed Mater Eng **14,** 439, 2004.
17. Saito, A., Taketani, S., Arai, K., Tanaka, M., Shimomura, M., and Sawa, Y. Highly regular honeycomb-patterned biodegradable scaffold promotes topographical control of myoblast proliferation and differentiation: A novel scaffold for myocardial regenerative therapy. J Mol Cell Cardiol **39,** 1022, 2005.
18. Tsuruma, A., Tanaka, M., Fukushima, N., and Shimomura, M. Morphological changes of neurons on self-organized honeycomb patterned films. Kobunshi Ronbunshu **61,** 628, 2004.
19. Tanaka, M., Tanakaya, A., Ito, E., Sunami, H., Yamamoto, S., and Shimomura, M. Effect of pore size of self-organized honeycomb-patterned polymer films on spreading, focal adhesion, proliferation, and function of endothelial cells. J Nanosci Nanotech in press.
20. Schwope, A.D., Wise, D.L., Sell, K.W., Dressler, D.P., and Skornick, W.A. Evaluation of wound-covering materials. J Biomed Mater Res **11,** 489, 1977.
21. Shimomura, M., Tanaka, M., Tsuruma, A., Sunami, H., and Yamamoto, S. Biomedical application of patterned polymer films prepared by self-organization. J Surf Sci Soc Jap **27,** 170, 2006.
22. Tsuruma, A., Tanaka, M., Fukushima, N., Yamamoto, S., and Shimomura, M. Morphological changes in neurons by self-organized patterned films. e-J Surf Sci Nanotech **3,** 159, 2005.

23. Tsuruma, A., Tanaka, M., Yamamoto, S., Fukushima, N., and Shimomura, M. Topographical control of neurites extension on stripe-patterned polymer films. Colloids Surf A Physicochem Eng Asp **284–285,** 548, 2006.
24. Fukuhira, Y., Kitazono, E., Hayashi, T., Kaneko, H., Tanaka, M., Shimomura, M., and Sumi, Y. Biodegradable honeycomb-patterned film composed of poly(lactic acid) and dioleoylphosphatidylethanolamine. Biomaterials **27,** 1797, 2006.
25. Yabu, H., Takebayashi, M., Tanaka, M., and Shimomura, M. Superhydrophobic and lipophobic properties of self-organized honeycomb and pincushion structures. Langmuir **21,** 3235, 2005.
26. Tanaka, Y., Sung, K.C., Tsutsumi, A., Ohba, S., Ueda, K., and Morrison, W.A. Tissue engineering skin flaps: which vascular carrier, arteriovenous shunt loop or arteriovenous bundle, has more potential for angiogenesis and tissue generation? Plast Reconstr Surg **112,** 1636, 2003.
27. Yabu, H., Tanaka, M., Ijiro, K., and Shimomura, M. Preparation of honeycomb-patterned polyimide films by self-organization. Langmuir **19,** 6297, 2003.
28. Butler, C.E., Orgill, D.P., Yannas, I.V., and Compton, C.C. Effect of keratinocyte seeding of collagen-glycosaminoglycan membranes on the regeneration of skin in a porcine model. Plast Reconstr Surg **101,** 1572, 1998.
29. McMillan, J.R., Akiyama, M., Nakamura, H., and Shimizu, H. Colocalization of multiple laminin isoforms predominantly beneath hemidesmosomes in the upper lamina densa of the epidermal basement membrane. J Histochem Cytochem **54,** 109, 2006.
30. Richardson, K.C., Jarret, L., and Finke, E.H. Embedding in epoxy resins for ultrathin sectioning in electron microscopy. Stain Technol **35,** 313, 1960.
31. Chometon, G., Zhang, Z.G., Rubinstein, E., Boucheix, C., Mauch, C., and Aumailley, M. Dissociation of the complex between cd151 and laminin-binding integrins permits migration of epithelial cells. Exp Cell Res 2006.
32. Patel, H., Marcelo, C., Voorhees, J.J., and Diaz, L.A. *In vitro* alterations of epidermal cell adhesion induced by temperature, substrate, and cations. J Invest Dermatol **76,** 474, 1981.
33. Rompre, P., Auger, F.A., Germain, L., Bouvard, V., Lopez Valle, C.A., Thibault, J., and Le Duy, A. Influence of initial collagen and cellular concentrations on the final surface area of dermal and skin equivalents: A Box-Behnken analysis. *In Vitro* Cell Dev Biol **26,** 983, 1990.
34. Presland, R.B., Kuechle, M.K., Lewis, S.P., Fleckman, P., and Dale, B.A. Regulated expression of human filaggrin in keratinocytes results in cytoskeletal disruption, loss of cell-cell adhesion, and cell cycle arrest. Exp Cell Res **270,** 199, 2001.
35. Lanschuetzer, C.M., Muss, W.H., Emberger, M., Pohla-Gubo, G., Klausegger, A., Bauer, J.W., and Hintner, H. Characteristic immunohistochemical and ultrastructural findings indicate that kindler's syndrome is an apoptotic skin disorder. J Cutan Pathol **30,** 553, 2003.
36. Jobard, F., Bouadjar, B., Caux, F., Hadj-Rabia, S., Has, C., Matsuda, F., Weissenbach, J., Lathrop, M., Prud'homme, J.F., and Fischer, J. Identification of mutations in a new gene encoding a FERM family protein with a pleckstrin homology domain in kindler syndrome. Hum Mol Genet **12,** 925, 2003.
37. Siegel, D.H., Ashton, G.H., Penagos, H.G., Lee, J.V., Feiler, H.S., Wilhelmsen, K.C., South, A.P., Smith, F.J., Prescott, A.R., Wessagowit, V., Oyama, N., Akiyama, M., Al Aboud, D., Al Aboud, K., Al Githami, A., Al Hawsawi, K., Al Ismaily, A., Al-Suwaid, R., Atherton, D.J., Caputo, R., Fine, J.D., Frieden, I.J., Fuchs, E., Haber, R.M., Harada, T., Kitajima, Y., Mallory, S.B., Ogawa, H., Sahin, S., Shimizu, H., Suga, Y., Tadini, G., Tsuchiya, K., Wiebe, C.B., Wojnarowska, F., Zaghloul, A.B., Hamada, T., Mallipeddi, R., Eady, R.A., McLean, W.H., McGrath, J.A., and Epstein, E.H. Loss of kindlin-1, a human homolog of the caenorhabditis elegans actin-extracellular-matrix linker protein unc-112, causes kindler syndrome. Am J Hum Genet **73,** 174, 2003.
38. Yamamoto, S., Tanaka, M., Sunami, H., Yamashita, S., Morita, Y., and Shimomura, M. Relationship between adsorbed fibronectin and cell adhesion on a honeycomb-patterned film. Surf Sci in press.
39. Yamamoto, S., Tanaka, M., Sunami, H., Yamashita, S., Morita, Y., and Shimomura, M. Relationship between adsorbed fibronectin and fak activation on a honeycomb-patterned film. J Surf Sci Soc Jap in press.
40. McKegney, M., Taggart, I., and Grant, M.H. The influence of crosslinking agents and diamines on the pore size, morphology and the biological stability of collagen sponges and their effect on cell penetration through the sponge matrix. J Mater Sci Mater Med **12,** 833, 2001.
41. Dai, N.T., Williamson, M.R., Khammo, N., Adams, E.F., and Coombes, A.G. Composite cell support membranes based on collagen and polycaprolactone for tissue engineering of skin. Biomaterials **25,** 4263, 2004.
42. Zhu, A.J. and Watt, F.M. Expression of a dominant negative cadherin mutant inhibits proliferation and stimulates terminal differentiation of human epidermal keratinocytes. J Cell Sci **109 (Pt 13),** 3013, 1996.
43. Takeichi, M., Watabe, M., Shibamoto, S., and Ito, F. Cadherin-dependent organization and disorganization of epithelial architecture. Princess Takamatsu Symp **24,** 28, 1994.
44. Akiyama, S.K., Larjava, H., and Yamada, K.M. Differences in the biosynthesis and localization of the fibronectin receptor in normal and transformed cultured human cells. Cancer Res **50,** 1601, 1990.
45. Kelly, T., Molony, L., and Burridge, K. Purification of two smooth muscle glycoproteins related to integrin. Distribution in cultured chicken embryo fibroblasts. J Biolog Chem **262,** 17189, 1987.
46. Srivastava, J., Elliott, B.E., Louvard, D., and Arpin, M. Src-dependent ezrin phosphorylation in adhesion-mediated signaling. Mol Biol Cell 2005.

Address reprint requests to:
James R. McMillan, M.Sc. Ph.D.
Department of Dermatology
Hokkaido University Graduate School of Medicine
North 15 West 7, Kitaku
Sapporo 060-8638, Japan

E-mail: jrm57@med.hokudai.ac.jp

ABSTRACT: Epidermolysis bullosa simplex with muscular dystrophy (EBS-MD, MIM 226670) is caused by plectin defects. We performed mutational analysis and immunohistochemistry using EBS-MD (n = 3 cases) and control skeletal muscle to determine pathogenesis. Mutational analysis revealed a novel homozygous plectin-exon32 rod domain mutation (R2465X). All plectin/HD1-121 antibodies stained the control skeletal muscle membrane. However, plectin antibodies stained the cytoplasm of type II control muscle fibers (as confirmed by ATPase staining), whereas HD1-121 stained the cytoplasm of type I fibers. EBS-MD samples lacked membrane (n = 3) but retained cytoplasmic HD1-121 (n = 1) and plectin staining in type II fibers (n = 3). Ultrastructurally, EBS-MD demonstrated widening and vacuolization adjacent to the membrane and disorganization of Z-lines (n = 2 of 3) compared to controls (n = 5). Control muscle immunogold labeling colocalized plectin and desmin to filamentous bridges between Z-lines and the membrane that were disrupted in EBS-MD muscle. We conclude that fiber-specific plectin expression is associated with the desmin-cytoskeleton, Z-lines, and crucially myocyte membrane linkage, analogous to hemidesmosomes in skin.

Muscle Nerve **35:** 24–35, 2007

PLECTIN DEFECTS IN EPIDERMOLYSIS BULLOSA SIMPLEX WITH MUSCULAR DYSTROPHY

J.R. McMILLAN, PhD,[1] M. AKIYAMA, PhD,[1] F. ROUAN, PhD,[2] J.E. MELLERIO, MD,[3] E.B. LANE, PhD,[4] I.M. LEIGH, MD,[5] K. OWARIBE, PhD,[6] G. WICHE, PhD,[7] N. FUJII, MD,[8] J. UITTO, PhD,[2] R.A.J. EADY, DSc (Med),[3] and H. SHIMIZU, PhD[1]

[1] Department of Dermatology, Hokkaido University Graduate School of Medicine, Kita-ku, Sapporo 060-8638, Japan
[2] Department of Dermatology and Cutaneous Biology, Jefferson Medical College, Philadelphia, Pennsylvania USA
[3] St. John's Institute of Dermatology, King's College, St Thomas's Hospital, London, United Kingdom
[4] Department of Cell Structure, Department of Anatomy and Physiology, University of Dundee, United Kingdom
[5] Center for Cutaneous Research, St. Bartholomew's and the Royal London School of Medicine and Dentistry, Queen Mary College, London, United Kingdom
[6] Biosystems, Human Informatics, Nagoya University, Nagoya, Japan
[7] Department of Molecular Cell Biology, University of Vienna, Vienna, Austria
[8] Department of Neurology, National Omuta Hospital, Fukuoka, Japan

Accepted 27 July 2006

Genetic defects in the epidermal expression of plectin are known to form the basis of at least three disease subtypes: a rare, mild form of dominant epidermolysis bullosa simplex (EBS) with mottled pigmentation,[19,20] a severe recessive form of epidermolysis bullosa associated with pyloric atresia and severe loss of skin,[5,30,33] and a recessive form of EBS associated with muscular dystrophy (EBS-MD).[11,25,29,43,45,47] In EBS-MD, plectin defects are thought to affect plasma membrane–cytoskeletal interactions in skin and muscle causing epidermal blistering and late-onset muscle weakness.[11,25,29,45]

Plectin is a large, 450–500 kDa, cytoplasmic protein that acts as a link between various cytoskeletal systems and cell junctions.[50] In skin, plectin links the basal cell keratin intermediate filaments to the transmembrane collagen XVII[21] and the $\beta 4$ integrin subunit of the $\alpha 6\beta 4$ integrin located in the hemidesmosome.[22,23] In many tissues and cultured cells, plectin interacts with several cytoskeletal systems: actin microfilaments, intermediate filaments, or microtubules.[50] Plectin in different cells and tissue has the ability to interact with multiple binding partners including intermediate filaments (keratin, desmin, and vimentin), actin microfilaments, microtubules, and specialized molecules at specific junctions such

Abbreviations: BSA, bovine serum albumen; CT, computerized tomography; EBS-MD, recessive epidermolysis bullosa simplex associated with muscular dystrophy; GEL, gelatin; MRI, magnetic resonance imaging; NGS, normal goat serum; PBS, phosphate-buffered saline; PCR, polymerase chain reaction; TBS, Tris-buffered saline

Key words: plectin; intermediate filament; muscle; Z-line; epidermolysis bullosa

Correspondence to: J. R. McMillan; e-mail: jrm57@med.hokudai.ac.jp

Published online 11 September 2006 in Wiley InterScience (www.interscience.wiley.com). DOI 10.1002/mus.20655

as vinculin and β1 integrin in striated muscle costamere attachment sites[17,39,40,48] and Rack1.[32,42]

Multiple plectin isoforms are expressed in a tissue-specific manner in mammalian cells and tissues derived from a single gene, *PLEC1*.[7,10,36] In the mouse, plectin is expressed in at least 14 different isoforms, mostly resulting in different splice variants of the actin binding amino-terminal exon 2.[10] However, a form of plectin lacking all or part of the central rod domain (exons 31/32) has been proposed in the rat, similar to the system controlling dystrophin muscle expression.[7] More recently, distinct functions for different plectin isoforms have come to light after determining specific plectin isoform subcellular localization.[36]

Precise and complete isoform expression patterns in various human tissues including muscle have yet to be determined. However, intriguingly, muscle fiber type-specific expression patterns of plectin were reported in clinically normal and diseased human skeletal muscle[11,39] and at costamere membrane attachment sites.[18] Initial reports of control muscle staining with HD1-121 antibody suggested that HD1-121 stained Z-lines in type I muscle fibers, whereas other plectin antibodies (including the 10F6 and 5B3 antibodies) showed variable staining at the membrane.[11] EBS-MD muscle demonstrated a loss of membrane HD1-121 antibody staining with an unusual residual expression of sarcomere staining.[11] Further studies using control and diseased muscle have shown that plectin and desmin intermediate filaments closely encircle sarcomeres, as well as link to the plasma membrane.[4,11,16,38,40,41,43] More recently, in normal rat muscle plectin was suggested to associate with desmin at both vinculin- and dystrophin-containing plasma membrane junctions.[17]

In human skin plectin antibodies show two major epidermal staining patterns. First, a combined dermal–epidermal junction and suprabasal cytoplasmic pattern is seen with the majority of plectin antibodies (including 10F6, 5B3, 6C6,[52] and IFAP300, the hamster plectin homolog[44]). A second, dermal–epidermal junction restricted staining pattern is seen with the HD1-121 and plectin 7A8 antibodies.[25,45] Staining with all these antibodies is severely reduced or absent in EBS-MD patients' skin.[25,45] The binding sites of the majority of plectin antibodies have been identified as lying within the central rod domain including the HD1-121 antigen[15] and various rat plectin antibodies.[8,9,51,52] We now report the precise ultrastructural expression of plectin in normal human and EBS-MD muscle tissue using the most informative of the current battery of plectin antibodies. We have also examined the expression of important integral muscle components such as dystrophin, desmin, and α actinin in EBS-MD muscle. The aim of this study was to describe the plectin antibody expression patterns together with critical structural elements in striated muscle to determine the structure of plectin, its precise location, and likely function in striated muscle.

MATERIALS AND METHODS

Tissue Samples. Muscle and skin biopsy samples were obtained from three EBS-MD patients whose cases have been previously described.[34,45] All samples were collected after the patient's consent was obtained, with the relevant institutional approval for experiments involving human material in accordance with the principles of the Helsinki Declaration of 1975.

The clinical, histopathological, ultrastructural, and immunohistochemical details of skin findings (excluding mutation data), limited muscle histology, and immunohistochemistry from Case 1 were previously included in the report by Smith et al. (patient D3).[15] Case 1 was a man aged 33 years who had suffered from widespread friction-induced blistering of his skin since just after birth. He subsequently developed progressive muscle weakness before the age of 2 years and then became confined to a wheelchair. The family was of Maltese origin and the parents were related. Blistering was noted around the hands, feet, scalp, and face as he grew, and he developed hoarseness due to scarring of the anterior commissure of the larynx. He developed early onset and progressive muscular dystrophy before the age of 2 years and computerized tomography (CT) and magnetic resonance imaging (MRI) showed him to have cerebellar and cerebral atrophy. This patient was previously shown to have absent muscle plectin staining as highlighted by the antibody HD1-121.[6] Mutational analysis for this patient was performed here and is reported below.

Case 2 was a 10-year-old, fourth female child of Italian parents who were first cousins. Previously, mutations in the plectin gene (5905del2/5905del2) together with skin immunohistochemistry and ultrastructural findings in this patient were reported by Mellerio et al.[29] Case 2 also presented with widespread trauma-induced blistering on her fingers, hands, feet, and face shortly after birth. She experienced stridor associated with supraglottic scarring and stenosis from the first few weeks of life and underwent a tracheostomy at the age of 20 months because of recurrent episodes of respiratory embarrassment. The two elder siblings in the family were

unaffected. A third child had suffered from blistering and apneic episodes from birth and had died at age 4 years from respiratory obstruction.

The third case was a 45-year-old Japanese wheelchair-bound man, previously described by Pulkkinen et al.,[34,43] including the homozygous 5866delC/5866delC mutation, clinical details, and skin immunohistochemical and ultrastructural findings.

Electron microscopy of the skin biopsy from each patient indicated that blistering arose as a result of rupture of the basal epidermal cells at a level that was just above the keratinocyte plasma membrane[28,29,45] and these changes were associated with previously reported hemidesmosome structural abnormalities.[28] Specifically, EBS-MD Cases 1 and 2 showed poor hemidesmosome inner plaque assembly and keratin intermediate filament linkage to the hemidesmosome plaque.[36]

Control muscle samples (n = 5, in total) from the flexor digitorum (n = 1), gastrocnemius muscle (n = 2), and from paraspinal column (n = 2) were obtained from routine surgical procedures. Quadriceps muscle from patients with EBS-MD (n = 3) were biopsied under anesthesia for diagnostic purposes. The biopsy samples were divided and fixed for electron microscopy; they were snap-frozen in Tissue-Tek OCT compound (Miles Diagnostic, Elkhart, IN) using isopentane cooled by liquid nitrogen for cryostat sectioning or cryofixed for immunoelectron microscopy.

Mutation Detection. Genomic DNA was isolated from peripheral blood cells from the patient (in Case 1) and his immediate family members, and DNA from unrelated healthy individuals was used as a control. DNA was subject to polymerase chain reaction (PCR) followed by automated nucleotide sequencing of the PCR products. PCR amplification of exon 32 that contained the mutation was performed with the following primer pairs as previously described by Pulkkinen et al.[34]: Ex32 II L: 5′ GCTAATACGCATCACTATAGGAACAGACCACCATGTTCCG CGAGCTGGCCGAGG 3′; Ex32 R: 5′ TCACTTCTCCTTGAGCGCGATCT 3′.

The PCR products were subjected to automated sequencing using 12 overlapping primers covering the entire coding sequence of exon 32. The mutation was detected with Ex32 12/12 primers: sense, 5′ CTCAAGGCTGAGGCGGAACT 3′; antisense, 5′ TCACCCACCAAAGCGATCC 3′.

Light Microscopy and Immunohistochemistry. Immunohistochemical staining was performed with modifications previously described by McMillan et al.[26] Muscle cryostat sections (5 μm) were collected and dried on 3-aminopropyltriethoxysilane (APES)–coated slides (Sigma, Poole, UK). Sections were fixed in acetone (−20°C) for 10 min before being washed in 0.1 M Dulbecco's phosphate-buffered saline (PBS). Primary antibodies were diluted in 0.3% w/v bovine serum albumen (BSA) (ICN, Poole, UK) in PBS and were incubated for 30 min at 37°C in a humidified chamber. The primary antibodies used included the anti-HD1 antigen HD1-121,[15] dilution 1 in 50, which recognizes two distinct plectin rod domain epitopes that are likely closely related in the folded, native protein[31]; 5B3 and 10F6 (neat), both mouse monoclonal antibodies raised against the rod domain of rat plectin (from G. Wiche, Vienna, Austria[8]); and 4B4 raised against the β1 integrin (Beckman-Coulter, High Wycombe, UK), used at 1 in 200. Three antibodies recognizing three dystrophin antibodies were used: NCL-DYST1, NCL-DYST2, and NCL-DYST3 against the rod-, carboxyl-, amino-terminal domains (neat, 1 in 10, and 1 in 40, respectively; Novocastra, Newcastle upon Tyne, UK). Novocastra also supplied antibodies to β spectrin, (1 in 100), merosin (1 in 50), and β dystroglycan (1 in 50). Other antibodies and antiserum included were: desmin monoclonal D33 (Dako, High Wycombe, UK) 1 in 200; polyclonal desmin and vimentin (Sigma) used at 1 in 20, BM-75.2 against α actinin (Sigma) used at 1 in 200; and mouse anti-vinculin IgG (Sigma) used at 1 in 100. The slides were washed in PBS for 10 min, dried, and blocked with normal rabbit or goat serum (Dako) for 5 min, depending on the secondary antibody.

Immunoperoxidase. Consecutive 5-μm transverse frozen sections of normal and EBS-MD muscle were fixed in cold acetone, and endogenous biotin activity was blocked using 0.1% hydrogen peroxide. The immunohistochemical technique used streptavidin-biotin complexes coupled to horseradish peroxidase with diaminobenzidine visualization.[2] For primary antibody details, see the previous section. The secondary antibody was rabbit antimouse peroxidase conjugated and was diluted 1 in 500 (Dako) or biotin conjugated goat antimouse (1 in 500) followed by peroxidase conjugated streptavidin (diluted 1 in 1,000). Routine enzyme histochemistry fiber typing was performed by staining with NADPH and ATPase preparations at pH 9.4, 4.6, and 4.3. All experiments included appropriate positive and negative controls and were performed in duplicate.

Immunofluorescence. The secondary antibody dilution was 1 in 500 in 0.3% BSA in PBS. The secondary

Table 1. Details of the patients having epidermolysis bullosa simplex with muscular dystrophy.

	Case 1	Case 2	Case 3
Patient age, origin, muscle biopsy site, parental relationship	Male, 33 y, Maltese origin, quadriceps biopsy, consanguineous	Female, 10 y, Italian origin, quadriceps biopsy, consanguineous	Male, 45 y, Japanese origin, thigh muscle biopsy, consanguineous
PLEC1 mutation/site	R2465X/R2465X* Exon 32	5905del2/5905del2 Exon 31	5866delC/5866delC Exon 31
References			
Mutation report	R2465X/R2465X*	Mellerio et al.[29]	Pulkkinen et al.[34]
Clinical report	Smith et al.[45]	Smith et al.[45]	Pulkkinen et al.[34]

* *Novel mutation detailed in this report.*

antibodies used were rabbit antimouse FITC (Dako) or goat antimouse FITC (Dako) and donkey antirabbit Texas red (Amersham, Amersham, UK) and goat antimouse Texas red (Amersham). The muscle and skin sections were incubated for 30 min at 37°C in a dark chamber and then washed in PBS. Sections were dried in the dark and mounted in a 10% PBS/glycerol anti-fade mountant. All experiments included appropriate positive and negative controls and were performed in duplicate.

Transmission Electron Microscopy. Control muscle specimens (gastrocnemius and flexor digitorum, n = 2) and EBS-MD muscle (n = 3) were cut, attached to an immovable cork surface, fixed in half-strength Karnovsky's fixative containing 2% formaldehyde and 2.5% glutaraldehyde,[18] and routinely processed as described by McMillan and Eady[27] for electron microscopy. Briefly, samples were washed in 0.067 M cacodylate buffer; osmium postfixation was in 1.3% osmium for 2 h at room temperature. Specimens were stained en bloc in 5% uranyl acetate in 50% ethanol (1 h), dehydrated in a graded ethanol series (15 min each), and embedded in TAAB 812 or Araldite resin with hard hardener (TAAB, Aldermaston, UK) via propylene oxide (two washes). Semithin and ultrathin sections were cut on a Reichert OMU-4 ultramicrotome (Leica, Milton Keynes, UK). Semithin sections (0.5 μm thick) were stained with azure II and methylene blue.[37] Ultrathin sections (60–90 nm) were collected on copper grids, stained in 50% alcoholic uranyl acetate and lead citrate, and examined in either a JOEL 100CX or Hitachi H7100 electron microscope with an accelerating voltage of 75 kV.

Immunoelectron Microscopy. Muscle cryofixation and cryosubstitution was carried out as previously described.[26] Briefly, control muscle samples (calf leg muscle and control flexor digitorum muscle, n = 2) were cut, cryoprotected, and plunged into liquid propane cooled by liquid nitrogen in a Leica KF 80 freeze plunging machine. The EBS-MD muscle sample was taken from the thigh leg muscle (Table 1).

Samples were then placed in methanol at −80°C for 3 days in either an AFS or a CS AUTO freeze substitution machine (Reichert, Depew, New York). The samples were embedded in Lowicryl K11M resin/methanol mixtures at −60°C for 4 days while the percentage of Lowicryl K11M resin mixture was increased. The samples were embedded in K11M resin while being polymerized under an ultraviolet light in a dry nitrogen atmosphere. The edges of the blocks were sectioned to check orientation and ultrastructure. Ultrathin sections of 90-nm thickness were collected on pioloform-coated nickel grids and stored for immunolabeling.

Labeling was carried out by floating the nickel grids on drops of buffer in a clean, humid chamber. The grids were incubated in PBS containing 5% normal goat serum (NGS), 1% gelatin (GEL), and 1% bovine serum albumin (BSA) for 30 min. Primary antibodies were diluted in 1% NGS, 1% GEL, 1% BSA in PBS for 1 h followed by four PBS washes. All gold-conjugated antibodies were diluted in 0.2 M Tris-buffered saline (TBS), pH 8.2, with 1% NGS, 1% GEL, and 1% BSA. The secondary antibodies were 5- or 15-nm gold-conjugated goat antimouse and 5- or 15-nm gold-conjugated goat antirabbit (Biocell, Cardiff, UK). The grids were washed twice in TBS and distilled water and stained with 2.5% uranyl acetate in 50% ethanol for 15 min and observed. For each control or EBS-MD sample a total of 7–10 blocks were examined.

RESULTS

Mutation Detection. DNA isolated from peripheral blood cells of the patient (Case 1) with EBS-MD (Fig. 1A) and his parents was subjected to mutation detection analysis. Proband DNA underwent direct nucleotide sequencing for the entire intron–exon borders of the plectin gene. Direct nucleotide sequencing of exon 32 PCR products

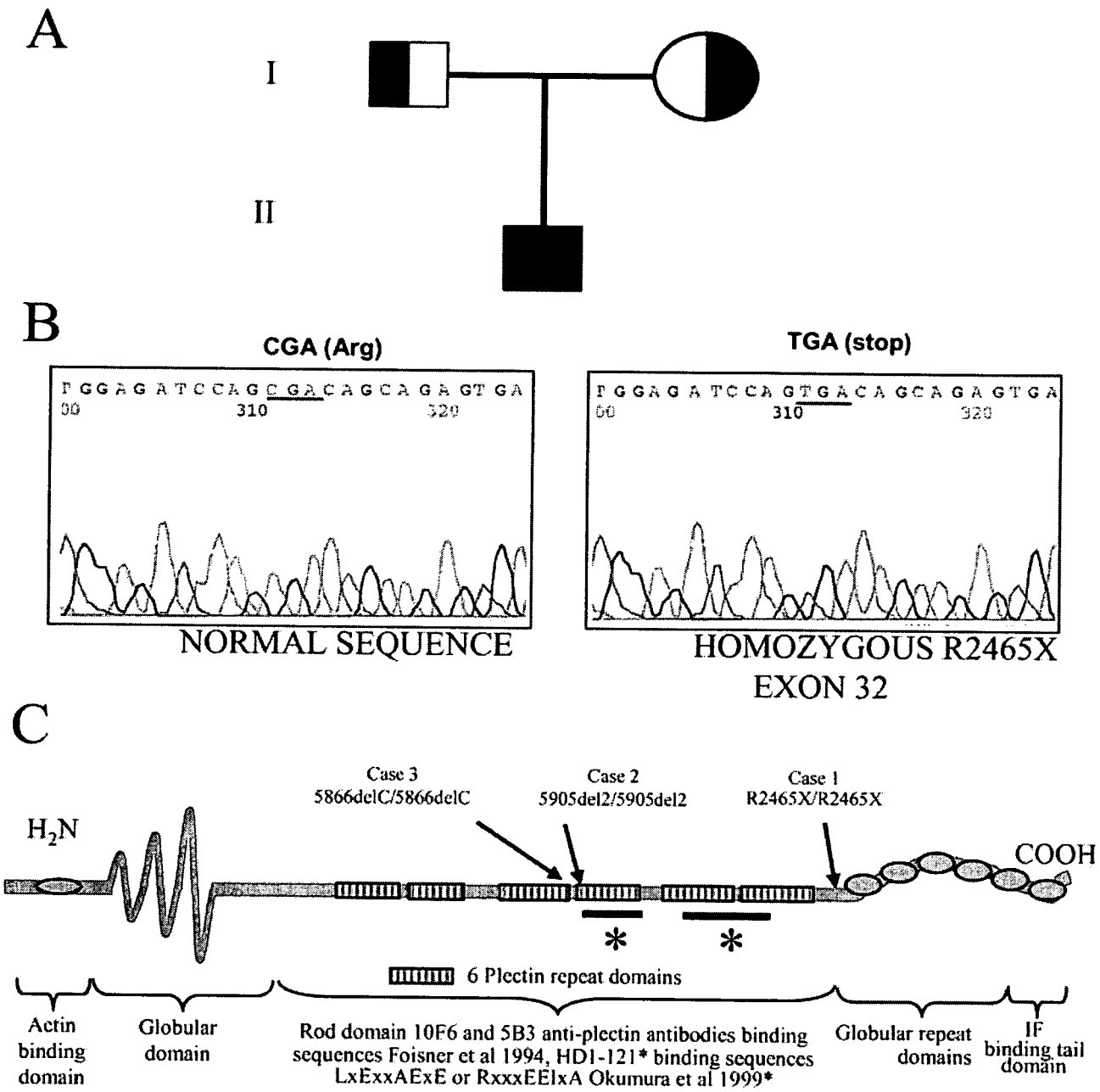

FIGURE 1. Mutation detection by automated nucleotide sequencing in a Maltese family with epidermolysis bullosa simplex and muscular dystrophy (EBS-MD). **(A)** Pedigree of the family from Case 1 with the proband suffering from EBS-MD. **(B)** Direct nucleotide sequencing of Ex32 PCR products revealed that the proband is homozygous for a C–T transition in nucleotide position 7444. This nucleotide substitution results in the change of an arginine residue (CAG) to a stop codon (TAG), and this mutation was designated R2465X. Predictions suggest that this mutation should lead to nonsense-mediated mRNA decay and a severe reduction or absence of plectin expression. **(C)** Summary of mutations in the three EBS-MD cases whose muscle findings are included in this report. Below, a schematic highlighting plectin domains and the binding sites of the three plectin antibodies (10F6/5B3/HD1-121) used in this study. The precise binding site in the rod domain of 5B3 and 10F6 antibodies is unknown (G. Wiche, personal communication).

revealed that the proband was homozygous for a C–T transition in nucleotide position 7444 when compared to unrelated, healthy individuals (n = 50). This nucleotide substitution resulted in a change of an arginine residue (CAG) to a stop codon (TAG), and this mutation was designated R2465X. We predict that this mutation will lead to nonsense-mediated mRNA decay and to a severe reduction or absence of plectin expression. The site of this mutation is at the very terminal, car-

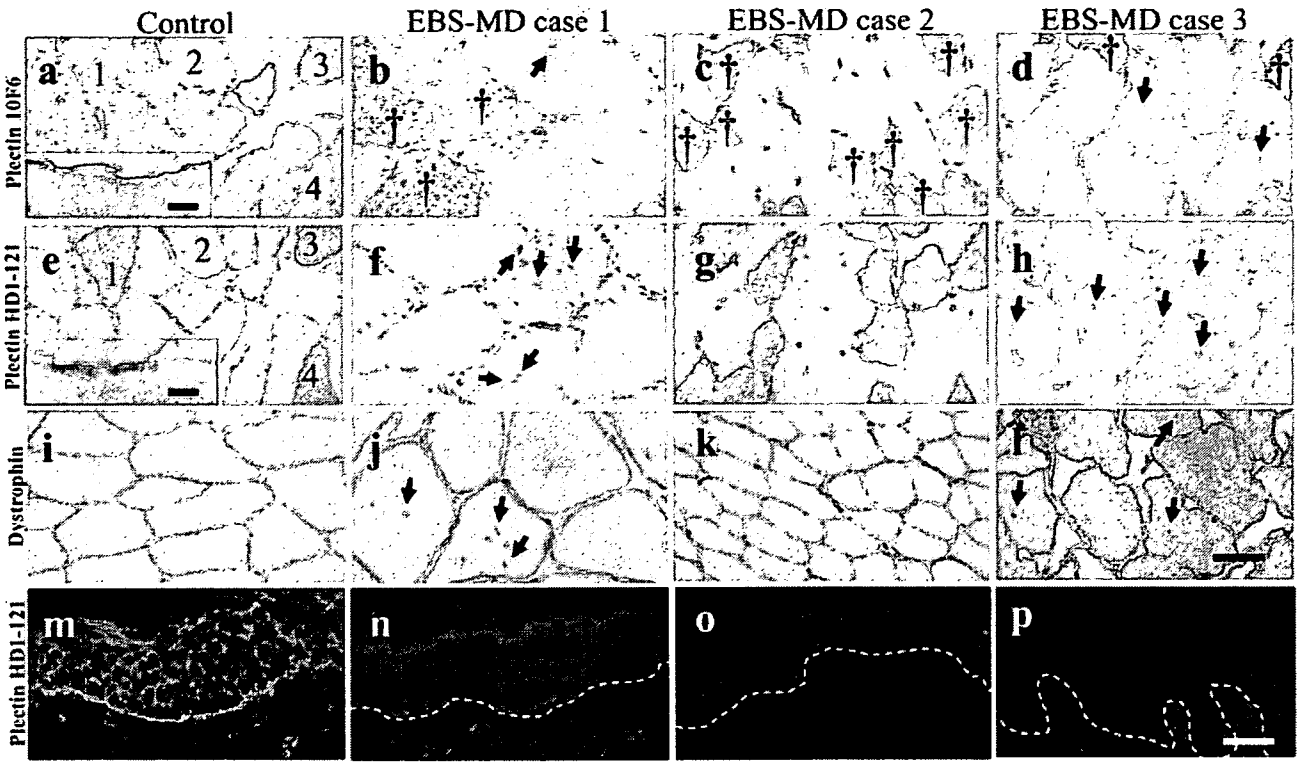

FIGURE 2. Loss of plectin expression at the periphery of all EBS-MD muscle fibers compared to control muscle myocytes. Plectin stained the membrane periphery of all control muscle fibers using all antibodies but only the center of selected fibers with the 10F6 antibody (**a** and inset) and the HD1-121 antibody (**e** and inset). However, plectin antibodies 10F6 **(b–d)** and HD1 **(f–h)** showed no staining at the cell periphery in all three EBS-MD patient muscle samples. In control type II muscle fibers, plectin (10F6) is expressed at the sarcolemma and within the cytoplasm but is restricted to the periphery of type I fibers. Conversely, plectin-HD1 is expressed at the periphery of all (type I and II) control muscle fibers but is restricted to the central cytoplasm of type I fibers. In EBS-MD muscle, plectin **(b–d)** and HD1 **(f–h)** expression is absent at the periphery of all muscle fibers. However, plectin expression is retained within the center of type II fibers in all EBS-MD cases together with multiple internalized nuclei (arrows). In comparison, HD1 was expressed in the center of type II fibers in only one case of EBS-MD muscle (Case 2, **g**). Thus, there is a profound reduction or loss of both plectin 10F6 and HD1-121 staining at the plasma membrane in EBS-MD tissue. In the youngest EBS-MD case **(g)** HD1 shows some cytoplasmic staining, but no staining occurs in the other cases **(f,h)**. Control muscle **(i)** and EBS-MD muscle **(j–l)**, showed normal peripheral dystrophin staining. Control skin showed linear staining **(m)** for plectin HD1-121, but in EBS-MD patients skin this staining was absent **(n–p)**. Inset **(a,e)** scale bar, 20 μm. Scale bar, 100 μm.

boxyl end of the rod domain that is encoded for by exon 32. Three different EBS-MD mutations in our patients' R2465X/R2465X (reported here for the first time, to our knowledge), 5866delC/5866delC, and 5905del2/5905del2 were located within the same plectin rod domain (Fig. 1C) and were all predicted to result in a severe reduction or ablation of full-length plectin expression in skin and skeletal muscle through nonsense-mediated mRNA decay. Any exon-specific plectin splicing involving the rod domain (as previously suggested[7,10,36]) could theoretically lead to some persistent plectin isoforms expression within certain organs and tissues.

Light Microscopy and Immunohistochemistry. Light microscope findings in Case 1 were previously reported briefly by us.[45] The appearances of the muscle biopsies particularly from the two oldest cases (Cases 1 and 3) were that of a chronic myopathy (Fig. 2b,d,f,h,j,l) sharing many of the histological features previously described.[3,45] There was wide variation in striated muscle-fiber size, the largest being hypertrophied, measuring more than 150–200 μm. There were both individual and grouped atrophic fibers. There were also increases in the amount of endomysial and perimysial connective tissue. Pyknotic nuclear clumps were present, and several fibers displayed multiple, internal nuclei (Fig. 2), as previously described.[45] There was evidence of continuing muscle-fiber necrosis: scattered fibers undergoing phagocytosis were observed and there were several hyaline (segmentally necrotic) myocytes. A few regenerating fibers were also observed. Case 3 also showed the formation of very small vacuoles at

the edge of occasional fibers that were not observed in Cases 1 or 2. Case 2, the youngest case included in this study, showed a very mild variation in myocyte fiber size but was otherwise unremarkable.

Immunoperoxidase. Plectin was localized in control muscle (using both 10F6 and 5B3 antibodies) to the membranes of both type I and type II fibers (Fig. 2a). Plectin was also expressed throughout the center of type II muscle fibers (see Fig. 2a), as defined by ATPase staining at pH 9.4, 4.6, and 4.3 (data not shown). This HD1-121 fiber type–specific finding was in agreement with the report of Gache et al.[11] In control muscle the majority (60%) of all muscle fibers exhibited staining for plectin within the center of the fibers. In EBS-MD Cases 1 and 3, plectin expression (using the same two antibodies) was completely absent from the plasma membrane and expressed in a speckled pattern within the center of 50%–60% of type II muscle fibers. Case 2 showed a similar loss of plectin immunoreactivity at the plasma membrane but a normal persistence of plectin expression within type II fibers (Fig. 2c).

Conversely, in control muscle the HD1 plectin antigen (recognized by the HD1-121 antibody) was expressed at the plasma membrane (Fig. 2e) of both type I and II muscle fibers. This showed similar staining patterns to previously reported plectin in muscle.[11] However, HD1 showed restricted expression within the center of type I fibers (see fibers with asterisks in Fig. 2e). HD1 antigen expression in the center of type II muscle cells was complementary (i.e., the exact reverse) of the plectin (10F5 and 5B3) staining observed in type I muscle fibers. Less than half of all control muscle fibers examined (between 30%–40%) exhibited this central HD1-121 staining pattern.

In EBS-MD muscle there was a loss of plasma membrane plectin and HD1 expression (in all plectin-deficient cases, Fig. 2f–h). In the majority of EBS-MD muscle (Cases 1 and 3, Figs. 2f,h) there was no HD1 expression within any of the muscle fibers except in Case 2 (Fig. 2g), where there was residual staining within the center of type I fibers. In control (Fig. 2i) and EBS-MD muscle (Fig. 2j–l), dystrophin stained the periphery of both types I and II muscle fibers. In all EBS-MD cases there was also a normal staining pattern for the integrin $\beta 1$ subunit, β spectrin, merosin, β dystroglycan, and vinculin similar to control muscle. Vimentin was expressed in selected muscle-fibers from EBS-MD cases 1 and 3 but not in control muscle.

Longitudinal muscle sections of α actinin and desmin staining (both Z-line–associated proteins) produced a regular banded pattern of staining in control muscle, but in EBS-MD muscle from Cases 1 and 3 this pattern was weak or severely, focally disrupted. An abnormal increase or clumping of α actinin and desmin staining was observed at the periphery of EBS-MD fibers in Case 1. Thus, the normal, striated pattern of the intermediate filament protein desmin (linking adjacent Z-lines and Z-lines to the plasma membrane) and α actinin, a structural protein and constituent of the Z-line, were disrupted in EBS-MD compared to control muscle.

Immunofluorescence. In control skin, bright, linear fluorescence was noted along the dermal–epidermal junction and within the cytoplasm of suprabasal keratinocytes (Fig. 2m) for plectin HD1-121, but in EBS-MD patients' skin this staining was completely absent (Fig. 2n–p). All other plectin antibodies including HD1-121, 10F6, 5B3, and 7A8[9] showed similar or identical skin staining patterns. This expression of plectin in EBS-MD skin was reported previously.[25,34,45]

Transmission Electron Microscopy. The most striking ultrastructural change in EBS-MD muscle was the increased space between the plasma membrane and the muscle sarcomere, seen in EBS-MD muscle (Fig. 3b,d) but not in controls (Fig. 3a). Case 1 (Fig. 3b) contained enlarged spaces between the folded plasma membrane and contractile units. This was a consistent finding in all five biopsy specimens. In addition, there was extensive reduplication of the basement membrane (Fig. 3b) caused by successive fiber necrosis and regeneration events. Small "focal densities" on the plasma membrane, associated with cytoskeletal filaments, were seen at regular intervals on the cytoplasmic surface of the plasma membrane in both control and EBS-MD muscle fibers (Fig. 3a, vs. 3b,d, respectively). The structure of these densities was unaffected by the muscle fiber pathology. Ultrastructural investigation of EBS-MD muscle from the youngest patient (Case 2, four samples) showed relatively mild myocyte disorganization and only very limited enlargement of the space between the membrane and the plasma membrane.

Comparison of control muscle (Fig. 3a) and EBS-MD muscle (Case 1, Fig. 3b,c; Case 3, Fig. 3d,e) revealed a focal loss of normal sarcomere organization in selected muscle fibers that appeared to resemble a fiber type–specific grouped pattern. However, the severe pathological changes in the EBS-MD muscle tissue made accurate ultrastructural fiber typing difficult (Fig. 3b–f). A further striking ultrastructural change in EBS-MD Cases 1 and 3 were the areas

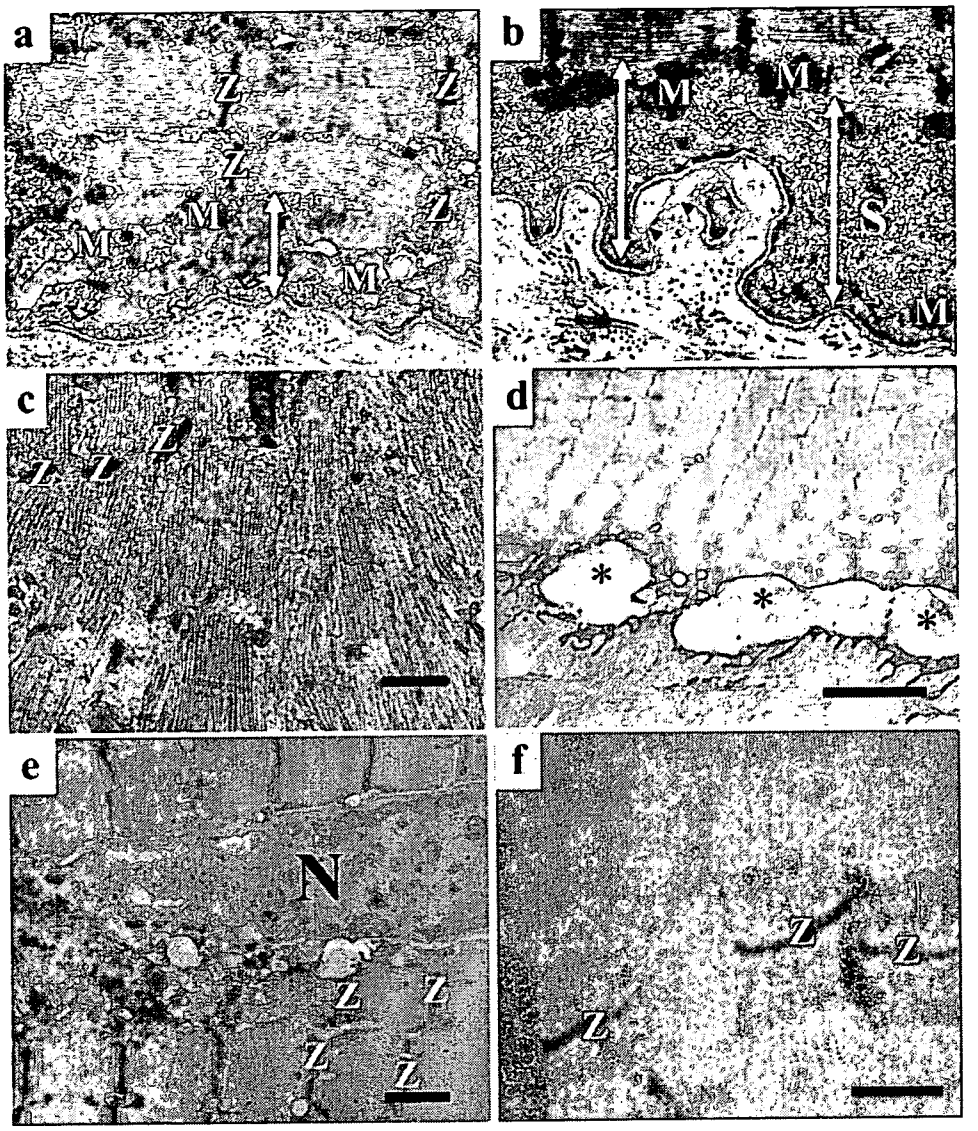

FIGURE 3. Muscle of patients with EBS-MD shows a severe loss of normal sarcomere organization and Z-line-plasma membrane anchorage. Transmission electron microscopy of muscle from normal control **(a)** and EBS-MD patients' muscle **(b–e)**. Compared to control muscle tissue **(a)**, EBS-MD muscle **(b)** shows a variably enlarged space (S, white arrow) between the plasma membrane and the muscle contractile units (sarcomeres). In both normal muscle **(a)** and EBS-MD Case 1 **(b)**, small electron densities were seen on the cytoplasmic surface of the plasma membrane (open arrows) **(a,b,d)**. Mitochondrial distributions within the normal parameter limits (M) were seen in the spaces beneath the plasma membrane both in normal and EBS-MD muscle. EBS-MD Case 1 also showed extensive basement membrane reduplication, suggesting that repetative fiber atrophy and regeneration had taken place **(b**, arrowheads). In a subset of myocytes there was focal loss of normal sarcomere organization **(c)** including the presence of small or disorganized Z-lines (Z) or a loss of Z-lines (asterisk, in **c**). In muscle from Case 3 **(d–f)**, similar sarcomere changes were present but in addition there were large vacuolated areas adjacent to the plasma membrane (asterisks in **d**). Within the center of muscle fibers in Case 3 there was a mild disorganized misalignment of sarcomeres and focal variability in Z-line size (Z in **e,f**). Abnormal, centrally located myocyte nuclei (N) were also observed **(e)**. Biopsies from Cases 1 and 3 both showed enlarged spaces between the myofibrillar apparatus and the myocyte plasma membrane and contained thin filaments that were possibly lost from the edge of the sarcomeres **(b,d)**. Scale bars: 1 μm **(a–c,e)**; 5 μm **(d)**; 0.5 μm **(f)**.

of focal myofibrillar disorganization. The loss of normal sarcomere organization was chiefly characterized by focal loss of or variation in normal Z-line size and alignment (Fig. 3). The width of the sarcomere unit and length of Z-lines were often thinner and smaller than controls (Fig. 3). This variation in Z-line size was beyond the normal variation observed in either type I or II fibers.[12,13] Where sarcomeres remained intact, they were incomplete or misaligned with their neighboring sarcomeres (Fig. 3b–f).

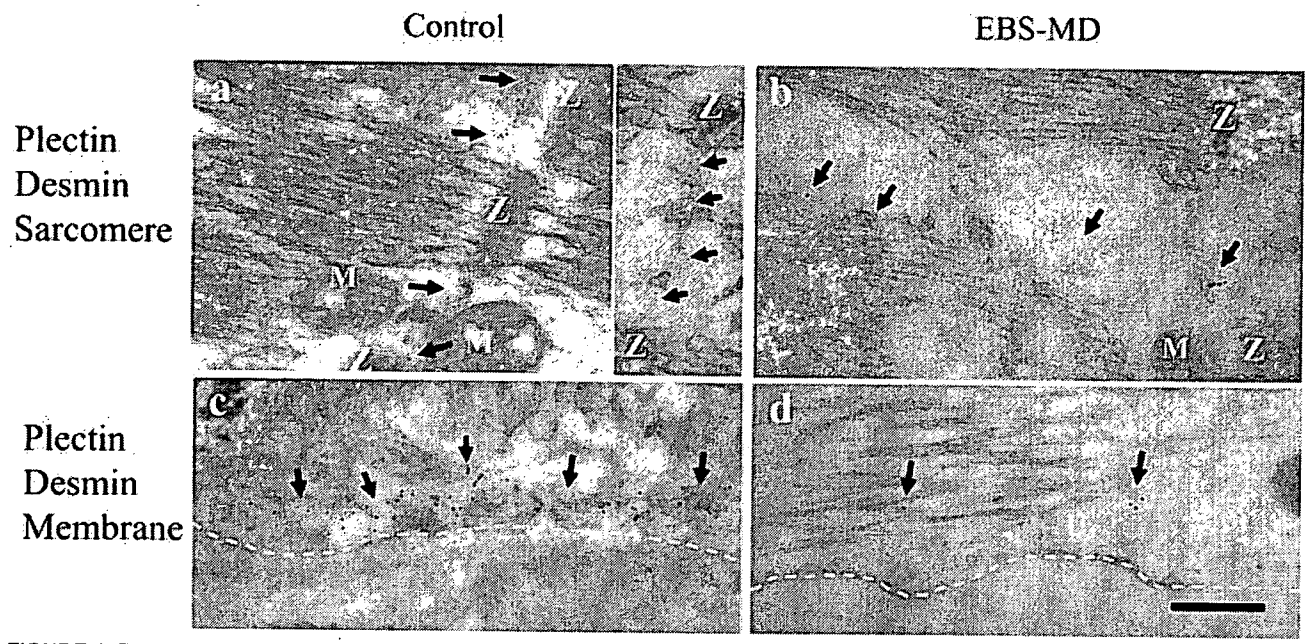

FIGURE 4. Plectin is coexpressed in control muscle with the intermediate filament protein desmin between adjacent Z-lines and between peripheral Z-lines and the plasma membrane, but this pattern is disrupted in plectin-deficient muscle. Double-labeling using immunogold electron microscopy in control muscle shows numerous plectin (5B3, small 5-nm gold particles) and desmin (larger 15-nm particles) labeling (arrows in **a**, and inset) adjacent to Z-lines (Z) but sparse labeling between Z-lines in EBS-MD muscle (arrows in **b**). In control muscle **(a)**, mitochondria (M) were regularly seen close to or adjacent to Z-lines (Z). In EBS-MD muscle (Case 3) Z-line plectin and desmin labeling **(b)** was severely reduced and disrupted compared to controls (see inset **b**). Furthermore, in control muscle significantly greater densities of plectin and desmin labeling were observed adjacent to the plasma membrane (arrows in **c**). In contrast, the periphery and plasma membrane of EBS-MD muscle showed significantly reduced plectin and desmin staining (arrows in **d**). Scale bar, 100 nm.

There was little uniformity between sarcomeres; thick and thin filaments could regularly be seen running at a tangent to the plasma membrane. The thick and thin filaments were observed at the edge of the sarcomere and often became extruded into the spaces between the sarcomeres (Fig. 3c). Z-line smearing was apparent in focal areas of sarcomere disorganization (Fig. 3c) but was not associated with any abnormal storage material within the myocyte. The loss of myofibrils was replaced by amorphous material, glycogen and swollen sarcoplasmic reticulum cisternae. The number and position of mitochondria at the cell periphery adjacent to the sarcomeres was within normal limits, occasionally showing a mild disruption in distribution in Cases 1 and 3.

Immunoelectron Microscopy. Double-labeling immunogold electron microscopy of control muscle fibers colocalized plectin (5B3) and desmin to between Z-lines (Fig. 4a,b). The muscle intermediate filament protein desmin showed a similar colocalization with HD1 in all fiber types. Mitochondria could be seen close to the Z-lines in control muscle (Fig. 4a). In EBS-MD muscle there was a severe loss or reduction and disruption in both plectin and desmin staining (Fig. 4b) compared to control muscle (Fig. 4a vs. 4b). Plectin and desmin colocalized to beneath the cytoplasmic face of small electron densities underlying the sarcolemma in control muscle (Fig. 4c), but in EBS-MD muscle there was a severe loss or reduction in this staining (Fig. 4d).

EBS-MD muscle also showed normal expression of all dystrophin antibody staining (including N- and C-terminal epitopes) in a regular fashion over small, discrete densities along the plasma membrane in a similar fashion to that observed in control muscle. Immunogold particle (5 nm) distribution along the plasma membrane demonstrated similar expression of the integrin $\beta 1$ subunit in control and EBS-MD muscle.

DISCUSSION

There are several major findings in this report. First, plectin (using all the plectin antibodies in this study) is expressed adjacent to the myocyte membrane in control type I and type II muscle fibers. However, multiple plectin antibodies show distinct fiber type–specific expression patterns within the center of normal type II muscle fibers. Conversely, staining for plectin with the HD1-121 antibody was restricted within the center of control type I muscle fibers.

From our data, we suggest that plectin or a closely related molecule is expressed in multiple fiber-specific isoforms comprising different rod domain sequences.[7,10] The significance of different plectin isoforms in at least these two subcellular locations, in the center of the muscle fiber between Z-lines and adjacent to the plasma membrane, is likely to be related to multiple crosslinking functions. In the center of the muscle fiber, plectin crosslinks the intermediate filaments desmin and vimentin (in regenerating fibers) running between Z-lines, and therefore might indirectly link Z-lines via interactions with components such as α actinin (a Z-line component).

At the muscle-fiber periphery, possible plectin-binding partners include desmin intermediate filaments, but also actin, vinculin, and α actinin at costamere β1 integrin-containing junctions.[38,40] The previously reported close association of plectin with costameres does not preclude it from association with dystrophin complex components; however, our data show no alterations in dystrophin proteins in EBS-MD muscle. In EBS-MD muscle there was a severe disruption in normal plectin, α actinin (a Z-line component), and desmin organization, suggesting that plectin is critical for normal sarcomere arrangement. Vimentin is an intermediate filament protein expressed in regenerating muscle, and was frequently observed in EBS-MD cases 1 and 3. Myocyte damage in plectin-deficient muscle may result from an uneven transfer of contractile energy between Z-lines and from Z-line to the myocyte costamere–plasma membrane via the desmin cytoskeleton. However, plectin may also play an additional role in supporting the normal vimentin-cytoskeleton during muscle-fiber regeneration. Plectin therefore might play multiple roles in EBS-MD pathogenesis.

In addition, plectin is thought to be responsible for maintaining the shape and mechanical stability of the myocyte between the Z-line and the myocyte plasma membrane.[14,24] Ultrastructurally, plectin- and desmin-deficient muscle share many similar features.[14,24] However, the loss of desmin was reported to cause more severe Z-line and sarcomere disruption than was seen in our plectin-deficient samples.[16]

A further significant finding was the loss of plectin staining from all EBS-MD patient tissue at the periphery of muscle fibers. Previously, plectin and HD1-121 had been reported present just within the myocyte membrane, and reduced or absent staining was reported in EBS-MD.[11] The colocalization of plectin and desmin intermediate filaments parallel to Z-lines suggests a role in the attachment and organizing of these structures. In addition, our studies colocalized plectin and desmin to the region immediately beneath the myocyte plasma membrane, which underlines the importance of anchorage between the cytoskeleton and the plasma membrane, analogous to hemidesmosomes in epithelia. In EBS-MD muscle the loss of membrane–intermediate filament connections via plectin caused increases in subsarcolemmal space and frequent juxtamembrane vacuolization, again highlighting the importance of cytoskeletal–plasma membrane anchorage in normal muscle.

A recently proposed role for desmin–mitochondrial interactions was not supported by a significant displacement of mitochondria in our EBS-MD muscle samples.[1,6,35] Proper uniform subcellular localization of mitochondria within the muscle fiber is essential for efficient energy transfer to the sarcomere, and hence correct muscle function, but may be a relatively minor contributing factor to the late-onset muscle weakness seen in EBS-MD.[35,36,46,49] However, we cannot rule out the possibility that a subtle redistribution of mitochondria may result in some loss of contractile capability in EBS-MD muscle. Further specific mitochondria staining and oxidative phosphorylation studies are required to investigate this.

From our data, it seems that plectin is vital in linking multiple proteins at different sites within muscle fibers to the cytoskeleton. Plectin deficiency in muscle has serious deleterious effects on the transmission of contractile forces from the adjacent sarcomeres via the desmin cytoskeleton to the plasma membrane and leads to the progressive pathological changes seen in this disorder. Elucidation of the full range of molecular interactions between plectin isoforms and the myocyte cytoskeleton will pave the way for a better understanding of the pathogenesis of EBS-MD and other muscular dystrophies.

Presented at the European Society for Dermatological Research and the Society for Investigative Dermatology, April 2004. We thank Dr. Jennian Geddes, Ms. Megumi Sato, and Dr. Osamu Shirado for significant contributions to this work. We thank Prof. D. Landon (Institute of Neurology, London) for comments and advice on this study. Supported by the Welcome Trust (to E.B.L., I.M.L., R.A.J.E.), the Muirhead Trust (to R.A.J.E.) and the Special Trustees of St. Thomas' Hospital (to R.A.J.E.), by a grant-in-aid for Scientific Research A (13357008, to H.S.) and a grant from the Japanese Health Science Foundation (to J.R.M., H.S.) and by a grant-in-aid from the Health and Labor Sciences Research Grant for research into specific diseases H17-Saisei-12 (to J.R.M.).

REFERENCES

1. Appaix F, Kuznetsov AV, Usson Y, Kay L, Andrienko T, Olivares J, et al. Possible role of cytoskeleton in intracellular arrangement and regulation of mitochondria. Exp Physiol 2003;88:175–190.